Supporting Information

Thermally-Activated Delayed Fluorescence Mediated Through the Upper Triplet State Manifold in non-Charge Transfer Star-Shaped Triphenylamine-Carbazole Molecules

Piotr Pander,[†] Radoslaw Motyka,[‡] Pawel Zassowski,[‡] Marc K. Etherington,[†] Daniele Varsano,[§] Tales J. da Silva,[∥] Marilia J. Caldas,[∥] Przemyslaw Data,*[†,‡,⊥] and Andrew P. Monkman [†]

[†] Department of Physics, Durham University, South Road, Durham, DH1 3LE, United Kingdom.

[‡] Faculty of Chemistry, Silesian University of Technology, Ks. M. Strzody 9, 44-100 Gliwice, Poland

[§] S3 Center, CNR Institute of Nanoscience, Modena, Italy

[∥] Institute of Physics, University of São Paulo, São Paulo, Brazil

[⊥] Centre of Polymer and Carbon Materials, Polish Academy of Sciences, M. Curie-Sklodowskiej 34, 41-819 Zabrze, Poland

Contents

1. Materials

Materials for the syntheses were purchased from Acros Organics, Sigma-Aldrich or POCH SA and used without further purification.

Melting points (not corrected) were determined in an open capillary [**OC**] or using a Boetius HMK apparatus [**B**];. ^{1}H and ^{13}C NMR spectra were recorded on a Varian 300 MHz System (300 MHz for ^{1}H, 75 MHz for ^{13}C), in a specified solvent and with tetramethylsilane as the internal reference. The chemical shifts (δ) are reported in parts per million (ppm) and the coupling constants (J) in Herz. Elemental analysis of the materials was carried out using Flash2000 (Thermofisher) apparatus. Materials were sublimed before use.

1.1. Synthesis of star-shaped tricarbazoylamines
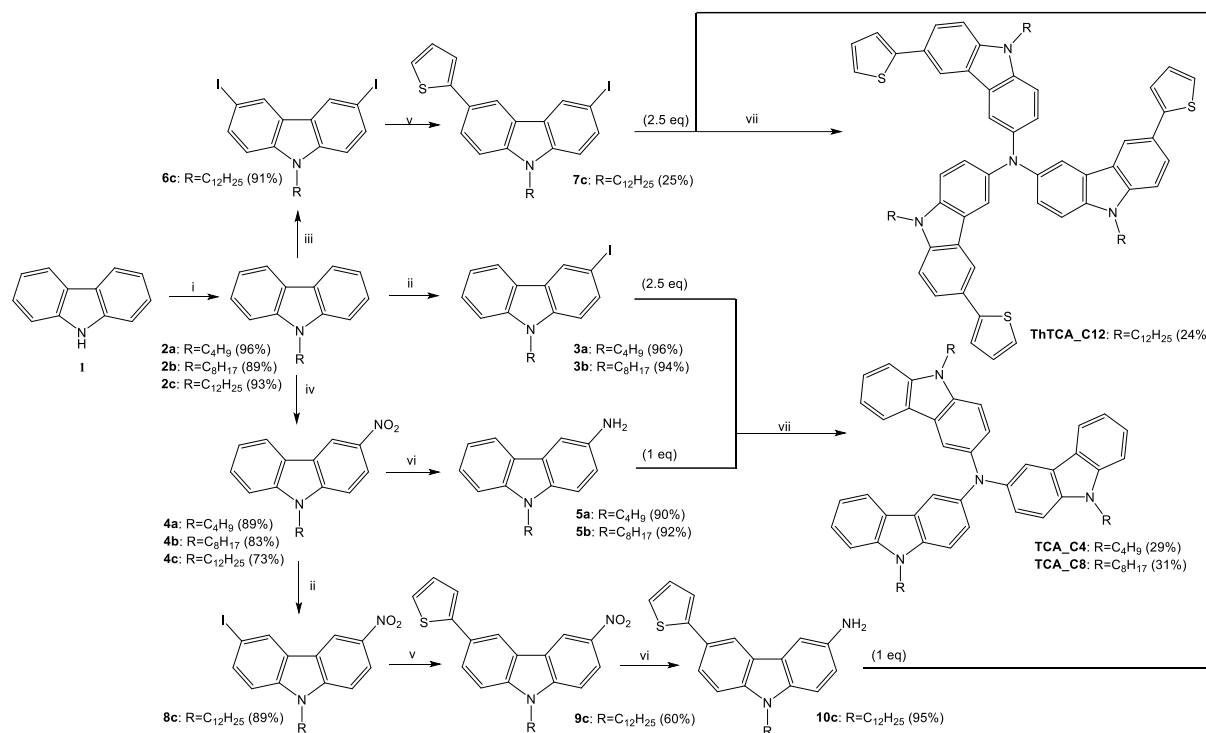
Scheme S1. Synthetic routes to tri(9-alkyl-9*H*-carbazol-3-yl)amines and their 6-substitued analogs. *Reagents and conditions:* **(i)** *RI, KOH, DMSO, r.t.;* **(ii)** *NIS (1 eq), CHCl$_3$:AcOH 4:1 v/v, r.t., 24 h;* **(iii)** *NIS (2.1 eq), CHCl$_3$:AcOH 4:1 v/v, r.t., 24 h;* **(iv)** *Cu(NO$_3$)$_2$•2.5H$_2$O (0.5 eq), AcOH:Ac$_2$O 1:2 v/v, r.t., 2 h;* **(v)** *2-TiB(OH)$_2$ (1 eq), Pd(PPh$_3$)$_2$, K$_2$CO$_2$ (2M), 70 °C, 24 h;* **(vi)** *Pd/C (10%), N$_2$H$_4$•H$_2$O, EtOH, reflux, 24 h;* **(vii)** *Pd$_2$(dba)$_3$, t-Bu$_3$PHBF$_4$, t-BuOK, benzene, reflux, 12 h.*

All products were synthesized starting from 9*H*-carbazole.

The main products **TCA_C4**, **TCA_C8** and **ThTCA_C12** were synthesized *via* a Buchwald-Hartwig cross-coupling reaction using the slightly modified procedure reported by Grazulevicius, Stakhira et al.[S1] Compounds **TCA_C4** and **TCA_C8** in which carbazole rings are not substituted at the 6-position were synthesized from the corresponding amino (**3**) and iodo (**5**) derivatives of 9-alkyl-9*H*-carbazole which can be relatively easy obtained from commercially available carbazole (Scheme 1). Compound **ThTCA_C12** where thiophene rings

were introduced to the tricarbazoylamine core required a slightly longer synthetic route (Scheme 1).

In the first step, 9*H*-carbazol was *N*-alkylated with alkyl iodides in DMSO, in the presence of KOH. Advantages of this method are the sufficiently high yields (**2a** – 96 %, **2b** – 89 % and **2c** – 93 %) and that non-anhydrous solvent can be used. The obtained *N*-alkylcarbazoles were converted by electrophilic substitution to the corresponding derivatives: reaction with N-iodosuccynimide (NIS) gave iodo **3a** (96 %), **3b** (94 %) and diiodo **6c** (91 %) compounds while nitration by $Cu(NO_3)_2$ in the mixture of acetic anhydride and acetic acid following the procedure reported by Kaya and Koyuncu[S2] yielded nitro derivatives **4a** (89 %), **4b** (83 %) and **4c** (73 %). Subsequent reduction of **4a** and **4b** gave appropriate amines **5a** (90 %) and **5b** (92 %), which together with **3a** and **3b** were used to obtain **TCA_C4** and **TCA_C8**.

For the synthesis of **ThTCA_C12,** it was necessary to introduce thiophene rings to the carbazole derivatives prior the Buchwald-Hartwig amination because tricarbazoylamines are unstable under the reaction conditions needed to enter them later. Compound **7c** (25 %) and **9c** (60 %) were synthetized *via* a Suzuki-Miyaura reaction of **8c** and **6c** respectively with 2-thienylboronic acid. Low yield of **7c** may be associated with the fact that this compound is probably more reactive towards 2-thienylboronic acids than starting substrate **6c** which is shown in obtaining significant amounts of disubstituted product namely 9-dodecyl-3,6-bis(thiophen-2-yl)-9*H*-carbazole. Derivative **7c** was also obtained using a Stille coupling reaction (not shown in the Scheme 1) according to the method published by Brzęczek et al.[S3] Because it did not result in significant improvement of reaction yield, further attempts to optimize the synthesis have been discontinued.

1.2.   Synthesis of 9-alkyl-9*H*-carbazoles (2).

Carbazole (1.67 g, 10.0 mmol) and powdered potassium hydroxide (0.84 g, 15.0 mmol) were mixed together in 50 cm^3 of DMSO under atmosphere of argon for 10 min. Then alkyl iodide

(9.95 mmol) was added dropwise with stirring. The reaction mixture became cloudy during the course of synthesis. The stirring was continued for 24 h at room temperature. Water (150 cm^3) was added to the reaction mixture and then precipitated solids were separated by filtration, rinsed with water and dried on air. Crude products were chromatographed on silica gel using hexane:dichloromethane (6:1 v/v) as an eluent. In the case when an oil, instead of a solid, separated after the addition of water, the reaction mixture was extracted with dichloromethane (3x50 cm^3), combined extracts were rinsed with water and dried over MgSO$_4$. A resulting solution was evaporated, and the residue was flash-chromatographed using the same eluents as before.

9-butyl-9H-carbazole (2a): butyl iodide 1.13 cm^3 (1.83 g, 9.95 mmol), yield 2.14 g (96 %), white solid, m.p. 56-58 °C (lit.4 55-57 °C); ^{1}H NMR (300 MHz, CDCl$_3$) δ: 0.91 (t, $^3J = 7.3$ Hz, 3H, -CH$_3$), 1.30-1.43 (m, 2H, -$\underline{CH_2}$-CH$_3$), 1.76-1.86 (m, 2H, -$\underline{CH_2}$-CH$_2$CH$_3$), 4.25 (t, $^3J = 7.1$ Hz, -CH$_2$-N), 7.21 (ddd, $^3J = 7.8$ Hz, $^3J = 6.9$ Hz, $^4J = 1.2$ Hz, 2H, C$_3$-H and C$_6$-H), 7.36-7.39 (m, 2H, C$_1$-H and C$_8$-H), 7.44 (ddd, $^3J = 8.1$ Hz, $^3J = 6.9$ Hz, $^4J = 1.2$ Hz, 2H, C$_2$-H and C$_7$-H), 8.09 (ddd, $^3J = 7.8$ Hz, $^4J = 1.2$ Hz, $^5J = 0.6$ Hz, 2H, C$_4$-H and C$_5$-H); ^{13}C-NMR (75 MHz, CDCl$_3$) δ: 14.0 (-CH$_3$), 20.7 (-$\underline{CH_2}$-CH$_3$), 31.2 (-$\underline{CH_2}$-CH$_2$CH$_3$), 42.9 (-CH$_2$-N), 108.8 (C$_1$, C$_8$), 118.8 (C$_3$, C$_6$), 120.4 (C$_4$, C$_5$), 122.9 (C$_{4a}$, C$_{4b}$), 128.7 (C$_2$, C$_7$), 140.6 (C$_{8a}$, C$_{9a}$).

9-octyl-9H-carbazole (2b): octyl iodide 2.39 g (9.95 mmol), yield 2.49 g (89%), colorless oil; ^{1}H NMR (300 MHz, CDCl$_3$) δ: 0.86 (t, $^3J = 6.9$ Hz, 3H, -CH$_3$), 1.20-1.40 (m, 10H), 1.80-1.89 (m, 2H), 4.27 (t, $^3J = 7.2$ Hz, -CH$_2$-N), 7.21 (ddd, $^3J = 7.8$ Hz, $^3J = 6.9$ Hz, $^4J = 1.2$ Hz, 2H, C$_3$-H and C$_6$-H), 7.36-7.41 (m, 2H, C$_1$-H and C$_8$-H), 7.45 (ddd, $^3J = 8.1$ Hz, $^3J = 6.9$ Hz, $^4J = 1.2$ Hz, 2H, C$_2$-H and C$_7$-H), 8.09 (ddd, $^3J = 7.8$ Hz, $^4J = 1.2$ Hz, $^5J = 0.6$ Hz, 2H, C$_4$-H and C$_5$-H); ^{13}C-NMR (75 MHz, CDCl$_3$) δ: 14.2 (-CH$_3$), 22.7, 27.5, 29.1, 29.3, 29.5, 31.9, 43.2 (-CH$_2$-N), 108.8 (C$_1$, C$_9$), 118.8 (C$_3$, C$_6$), 120.4 (C$_4$, C$_5$), 123.0 (C$_{4a}$, C$_{4b}$), 125.7 (C$_2$, C$_7$), 140.6 (C$_{8a}$, C$_{9a}$).

9-dodecyl-9H-carbazole (2c): dodecyl iodide 2.95 g (2.46 cm^3, 9.95 mmol), yield 3.12 g (93%), white waxy solid, m.p. 46-48 °C; ^{1}H NMR (300 MHz, CDCl$_3$) δ: 0.87 (t, ^3J = 6.7 Hz, 3H, -CH$_3$), 1.14-1.46 (m, 18H), 1.80-1.90 (m, 2H), 4.28 (t, ^3J = 7.3 Hz, -CH$_2$-N), 7.21 (ddd, ^3J = 7.8 Hz, ^3J = 6.9 Hz, ^4J = 1.2 Hz, 2H, C$_3$-H and C$_6$-H), 7.35-7.42 (m, 2H, C$_1$-H and C$_8$-H), 7.46 (ddd, ^3J = 8.1 Hz, ^3J = 6.9 Hz, ^4J = 1.2 Hz, 2H, C$_2$-H and C$_7$-H), 8.10 (ddd, ^3J = 7.8 Hz, ^4J = 1.2 Hz, ^5J = 0.6 Hz, 2H, C$_4$-H and C$_5$-H); ^{13}C-NMR (75 MHz, CDCl$_3$) δ: 14.3 (-CH$_3$), 22.8, 27.5, 29.1, 29.5, 29.6, 29.7, 29.7, 29.7, 29.8, 31.9, 43.2 (-CH$_2$-N), 108.8 (C$_1$, C$_9$), 118.8 (C$_3$, C$_6$), 120.5 (C$_4$, C$_5$), 123.0 (C$_{4a}$, C$_{4b}$), 125.7 (C$_2$, C$_7$), 140.6 (C$_{8a}$, C$_{9a}$).

1.3. Synthesis of 9-alkyl-3-iodo-9*H*-carbazoles (3).

A mixture of **2** (10.0 mmol) and *N*-iodosuccinimide (NIS) (2.25 g, 10.0 mmol) was stirred overnight in chloroform (100 cm^3) and acetic acid (30 cm^3) at room temperature, under atmosphere of argon. The reaction mixture was then poured into water and the organic phase was separated, washed with 50 cm^3 of 5% sodium bicarbonate solution and then once more with 50 cm^3 of water. The organic layer was dried over MgSO$_4$ and filtered. Removal of the solvent followed by column chromatography on silica gel using hexane/dichloromethane (6/1) as an eluent afforded **3** as an oil solidifying with time.

9-butyl-3-iodo-9H-carbazole (3a): From **2a** 2.23 g (10.0 mmol), yield 3.35 g (96%), solidifying with time oil; ^{1}H NMR (300 MHz, CDCl$_3$) δ: 0.91 (t, ^3J = 7.3 Hz, 3H, -CH$_3$), 1.29-1.42 (m, 2H, -CH$_2$-CH$_3$), 1.76-1.86 (m, 2H, -CH$_2$-CH$_2$CH$_3$), 4.24 (t, ^3J = 7.2 Hz, -CH$_2$-N), 7.16 (d, ^3J = 8.7 Hz, 1H, C$_1$-H), 7.19-7.26 (m, 1H, C$_6$-H), 7.38 (d, ^3J = 7.5 Hz, 1H, C$_8$-H), 7.43-7.50 (m, 1H, C$_7$-H), 7.67 (dd, ^3J = 8.7 Hz, ^4J = 1.8 Hz, 1H, C$_2$-H), 7.99-8.04 (m, 1H, C$_5$-H), 8.38 (d, ^4J = 1.8 Hz, 1H, C$_4$-H); ^{13}C-NMR (75 MHz, CDCl$_3$) δ: 14.0 (-CH$_3$), 20.6 (-CH$_2$-CH$_3$), 31.1 (-CH$_2$-CH$_2$CH$_3$), 43.0 (-CH$_2$-N), 81.2 (C$_3$-I), 109.0 (C$_8$), 110.9 (C$_1$), 119.4 (C$_6$), 120.6 (C$_5$), 121.7 (C$_{4b}$), 125.5 (C$_{4a}$), 126.4 (C$_7$), 129.3 (C$_2$), 133.9 (C$_4$), 139.7 (C$_{9a}$), 140.5 (C$_{8a}$).

3-iodo-9-octyl-9H-carbazole (3b): From **2b** 2.79g (10.0 mmol), yield 3.81 g (94%) of an oil, solidifying with time, m.p. was not determined; ^{1}H NMR (300 MHz, CDCl$_3$) δ: 0.85 (t, ^3J = 7.2 Hz, 3H, -CH$_3$), 1.15-1.40 (m, 10H), 1.75-1.88 (m, 2H), 4.23 (t, ^3J = 7.2 Hz, -CH$_2$-N), 7.17 (d, ^3J = 8.6 Hz, 1H, C$_1$-H), 7.19-7.26 (m, 1H, C$_6$-H), 7.35-7.41 (m, 1H, C$_8$-H), 7.44-7.51 (m, 1H, C$_7$-H), 7.68 (dd, ^3J = 8.6 Hz, ^4J = 1.8 Hz, 1H, C$_2$-H), 8.03 (ddd, ^3J = 7.8 Hz, ^4J = 1.2 Hz, ^5J = 0.6 Hz, 2H, C$_5$-H), 8.38 (dd, ^4J = 1.8 Hz, ^5J = 0.6 Hz, 1H, C$_4$-H); ^{13}C-NMR (75 MHz, CDCl$_3$) δ: 14.2 (-CH$_3$), 22.7, 27.4, 29.0, 29.2, 29.5, 31.9, 43.3 (-CH$_2$-N), 81.2 (C$_3$-I), 109.0 (C$_8$), 110.9 (C$_1$), 119.4 (C$_6$), 120.6 (C$_5$), 121.7 (C$_{4b}$), 125.5 (C$_{4a}$), 126.4 (C$_7$), 129.3 (C$_2$), 133.9 (C$_4$), 139.7 (C$_{9a}$), 140.5 (C$_{8a}$).

1.4.   Synthesis of 9-alkyl-3-nitro-9*H*-carbazoles (4).

Cu(NO$_3$)$_2$•2.5H$_2$O (2.33 g, 10.0 mmol) was slowly added to a mixture of **2** (20.0 mmol) in acetic acid (25 cm^3) and acetic anhydride (50 cm^3) at room temperature. Then 15 cm^3 of acetic acid was added to the reaction mixture. The reaction was vigorously stirred. After 1.5 h it was poured onto distilled water (500 cm^3). The yellow precipitate was collected by filtration, washed three times with water (300 cm^3), and dried under vacuum. Crude products were chromatographed on silica gel using hexane:chloroform (2:1 v/v) as an eluent.

9-butyl-3-nitro-9H-carbazole (4a): From **2a** 4.46 g (20.0 mmol), yield 4.78 g (89%), yellow crystals, m.p. 94-96 °C; ^{1}H NMR (300 MHz, CDCl$_3$) δ: 0.96 (t, ^3J = 7.3 Hz, 3H, -CH$_3$), 1.33-1.49 (m, 2H, , -C$\underline{H}_2$-CH$_3$), 1.81-1.90 (m, 2H, -C$\underline{H}_2$-CH$_2$CH$_3$), 4.34 (t, ^3J = 7.2 Hz, 2H, -CH$_2$-N-), 7.35 (ddd, ^3J = 7.9 Hz, ^3J = 7.1 Hz, ^4J = 1.2 Hz, 1H, C$_6$-H), 7.40 (d, ^3J = 9.1 Hz, 1H, C$_1$-H), 7.44-7.50 (m, 1H, C$_8$-H), 7.57 (ddd, ^3J = 7.9 Hz, ^3J = 7.1 Hz, ^4J = 1.2 Hz, 1H, C$_7$-H), 8.14 (ddd, ^3J = 7.8 Hz, ^4J = 1.2 Hz, ^5J = 0.9 Hz, 1H, C$_5$-H), 8.37 (dd, ^3J = 9.1 Hz, ^4J = 2.3 Hz, 1H, C$_2$-H), 9.00 (d, ^4J = 2.3 Hz, 1H, C$_4$-H). ^{13}C-NMR (75 MHz, CDCl$_3$) δ: 13.9 (-CH$_3$), 20.6 (-C$\underline{H}_2$-CH$_3$), 31.2 (-C$\underline{H}_2$-CH$_2$CH$_3$), 43.5 (-CH$_2$-N), 108.4, 109.8, 117.4, 120.8, 121.1, 121.7, 122.7, 123.0, 127.5, 140.7 (C$_3$), 141.8, 143.6.

3-nitro-9-octyl-9H-carbazole (4b): From **2b** 5.59 g (20.0 mmol), yield 5.38 g (83%), yellow

crystals, m.p. 83-85 °C, ^{1}H NMR (300 MHz, CDCl$_3$) δ: 0.85 (t, ^3J = 7.0 Hz, 3H, -CH$_3$), 1.14-

1.44 (m, 10H), 1.80-1.93 (m, 2H), 4.30 (t, ^3J = 7.5 Hz, 2H, -CH$_2$-N-), 7.29-7.37 (m, 1H, C$_6$-H),

7.36 (d, ^3J = 9.0 Hz, 1H, C$_1$-H), 7.45 (d, ^3J = 8.2 Hz, 1H, C$_8$-H), 7.56 (ddd, ^3J = 8.2 Hz, ^3J = 7.1

Hz, ^4J = 1.2 Hz, 1H, C$_7$-H), 8.11 (d, ^3J = 7.8 Hz, C$_5$-H), 8.35 (dd, ^3J = 9.0 Hz, ^4J = 2.3 Hz, 1H,

C$_2$-H), 8.95 (d, ^4J = 2.3 Hz, 1H, C$_4$-H). ^{13}C-NMR (75 MHz, CDCl$_3$) δ: 14.2 (-CH$_3$), 22.7 (-C̲H̲$_2$-

CH$_3$), 27.3, 29.0, 29.2, 29.4, 31.8, 43.7 (-CH$_2$-N), 108.3, 109.8, 117.4, 120.8, 121.0, 121.6,

122.6, 122.9, 127.4, 140.6 (C$_3$), 141.7, 143.6.

9-dodecyl-3-nitro-9H-carbazole (4c): From **2c** 6.71 g (20.0 mmol), yield 5.56 g (73%), light

yellow crystals, m.p. 88-89 °C; ^{1}H NMR (300 MHz, CDCl$_3$) δ: 0.87 (t, ^3J = 6.7 Hz, 3H, -CH$_3$),

1.14-1.46 (m, 18H), 1.80-1.90 (m, 2H), 4.34 (t, ^3J = 7.2 Hz, 2H, -CH$_2$-N-), 7.30-7.39 (m, 1H,

C$_6$-H), 7.40 (d, ^3J = 9.0 Hz, 1H, C$_1$-H), 7.45-7.50 (m, 1H, C$_8$-H), 7.54-7.60 (m, 1H, C$_7$-H), 8.16

(ddd, ^3J = 7.8 Hz, ^4J = 1.2 Hz, ^5J = 0.6 Hz, 1H, C$_5$-H), 8.39 (dd, ^3J = 9.1 Hz, ^4J = 2.3 Hz, 1H,

C$_2$-H), 9.02 (d, ^4J = 2.3 Hz, 1H, C$_4$-H). ^{13}C-NMR (75 MHz, CDCl$_3$) δ: 14.3 (-CH$_3$), 22.8, 27.4,

29.2, 29.5, 29.6, 29.7, 29.7, 29.7, 29.8, 32.0, 43.8 (-CH$_2$-N), 108.4, 109.8, 117.5, 120.9, 121.1,

121.8, 122.7, 123.0, 127.5, 140.7 (C$_3$), 141.8, 143.7.

1.5. Synthesis of 9-alkyl-3-amino-9*H*-carbazoles (5).

Pd/C (10% w/w) (0.02 g) was added to the solution of **4** (15.0 mmol) in 300 cm^3 ethanol at

room temperature. Next the mixture was refluxed for 10 min. Then, 10 cm^3 of hydrazinium

hydroxide was added dropwise to the solution during 2 h. The mixture was stirred at reflux for

18 h and then the Pd on carbon was filtered off. Ethanol and hydrazinium hydroxide were

stripped by a rotary evaporator and the remaining solid was chromatographed on neutralized by

triethylamine silica gel using hexane:EtOAc (2:1 v/v) with 1% of TEA as an eluent.

3-amino-9-butyl-9H-carbazole (5a): From **4a** 4.02g (15.0 mmol), yield 3.22 g (90%), off-white

solid; ^{1}H NMR (300 MHz, CDCl$_3$) δ: 0.92 (t, ^3J = 7.3 Hz, 3H, -CH$_3$), 1.30-1.43 (m, 2H, , -C̲H̲$_2$-

CH$_3$), 1.75-1.86 (m, 2H, -CH$_2$-CH$_2$CH$_3$), 3.40 (br. s, 2H, -NH$_2$), 4.22 (t, ^3J = 7.2 Hz, 2H, -CH$_2$-N), 6.90 (dd, ^3J = 8.5 Hz, ^4J = 2.3 Hz, 1H, C$_2$-H), 7.11-7.17 (m, 1H), 7.21 (dd, ^3J = 8.5 Hz, ^4J = 0.6 Hz, 1H, C$_1$-H), 7.30-7.35 (m, 1H), 7.38-7.44 (m, 2H), 7.98 (ddd, ^3J = 7.8 Hz, ^4J = 1.2 Hz, ^5J = 0.6 Hz, 1H, C$_4$-H); ^{13}C-NMR (75 MHz, CDCl$_3$) δ: 14.0 (-CH$_3$), 20.7 (-CH$_2$-CH$_3$), 31.3 (-CH$_2$-CH$_2$CH$_3$), 43.0 (-CH$_2$-N), 106.4, 108.7, 109.3, 115.6, 118.1, 120.4, 122.4, 123.7, 125.5, 135.2, 139.0, 141.0.

3-amino-9-octyl-9H-carbazole (5b): From **4b** 4.87 g (15.0 mmol), yield 4.06 g (92%), off-white solid; ^{1}H NMR (300 MHz, CDCl$_3$) δ: 0.86 (t, ^3J = 6.8 Hz, 3H, -CH$_3$), 1.13-1.44 (m, 10H), 1.75-1.89 (m, 2H), 3.61 (br. s, 2H, -NH$_2$), 4.22 (t, ^3J = 7.2 Hz, 2H, -CH$_2$-N), 6.90 (dd, ^3J = 8.5 Hz, ^4J = 2.3 Hz, 1H, C$_2$-H), 7.11-7.17 (m, 1H), 7.21 (dd, ^3J = 8.5 Hz, ^4J = 0.6 Hz, 1H, C$_1$-H), 7.30-7.36 (m, 1H), 7.37-7.47 (m, 2H), 7.99 (ddd, ^3J = 7.8 Hz, ^4J = 1.2 Hz, ^5J = 0.6 Hz, 1H, C$_4$-H); ^{13}C-NMR (75 MHz, CDCl$_3$) δ: 14.2 (-CH$_3$), 22.7, 27.5, 29.2, 29.3, 29.5, 31.9, 43.3 (-CH$_2$-N), 106.4, 108.7, 109.3, 115.7, 118.0, 120.4, 122.4, 123.7, 125.5, 135.2, 139.0, 141.0.

1.6. Synthesis of *3,6-diiodo-9-dodecyl-9H-carbazoles (6c):*

Compound **6c** was obtained by the same procedure as **3a** except that NIS was used in an amount of 2 eq (4.50 g 20 mmol) relative to the substrate **2c** (3.35 g, 10mmol), yield 5.35 g (91%), white waxy solid; ^{1}H NMR (300 MHz, CDCl$_3$) δ: 0.87 (t, ^3J = 6.8 Hz, 3H, -CH$_3$), 1.13-1.38 (m, 18H), 1.67-1.87 (m, 2H), 4.18 (t, ^3J = 7.2 Hz, 2H, -CH$_2$-N), 7.14 (d, ^3J = 8.6 Hz, 2H, C$_1$-H and C$_8$-H), 7.69 (dd, ^3J = 8.6 Hz, ^4J = 1.7 Hz, 2H, C$_2$-H and C$_7$-H), 8.30 (d, ^4J = 1.7 Hz, 2H, C$_4$-H and C$_5$-H); ^{13}C-NMR (75 MHz, CDCl$_3$) δ: 14.3 (-CH$_3$), 22.8, 27.3, 28.9, 29.4(2xC), 29.6, 29.6, 29.7 (2xC), 32.0, 43.4 (-CH$_2$-N), 81.8 (C$_3$-I and C$_6$-I), 111.0 (C$_1$ and C$_8$), 124.1 (C$_{4a}$ and C$_{4b}$), 129.5 (C$_2$ and C$_7$), 134.6 (C$_4$ and C$_5$), 139.6 (C$_{8a}$ and C$_{9a}$).

Synthesis of *9-dodecyl-3-iodo-6-nitro-9H-carbazoles (8c):* Compound **8c** was obtained by the same procedure as **3a** except that **4c** (3.80 g, 10.0 mmol) was used instead of **2a**, yield 4.50 g (89%), light yellow solid; ^{1}H NMR (300 MHz, CDCl$_3$) δ: 0.87 (t, ^3J = 6.7 Hz, 3H, -CH$_3$), 1.13-

1.42 (m, 18H), 1.80-1.90 (m, 2H), 4.31 (t, $^3J = 7.2$ Hz, 2H, -CH$_2$-N), 7.25 (d, $^3J = 8.6$ Hz, 1H, C$_1$-H), 7.40 (d, $^3J = 9.1$ Hz, 1H, C$_8$-H), 7.80 (dd, $^3J = 8.6$ Hz, $^4J = 1.7$ Hz, 1H, C$_2$-H), 8.39 (dd, $^3J = 9.1$ Hz, $^4J = 2.3$ Hz, 1H, C$_7$-H), 8.45 (d, $^4J = 1.7$ Hz, 1H, C$_4$-H), 8.94 (d, $^4J = 2.3$ Hz, 1H, C$_5$-H).

1.7. Suzuki-Miyaura coupling – general procedure for 7c and 9c.

The reaction mixture of **6c** or **8c** (10.0 mmol), 1.28 g (10.0 mmol) 2-thienylboronic acid, 0.28 g (0.2 mmol) Pd(PPh$_3$)$_4$, 10 cm^3 2M K$_2$CO$_3$ (20.0 mmol) in 60 cm^3 degassed THF was stirred for 24 h at 70 °C under atmosphere of argon. The post-reaction mixture was diluted with water (150 cm^3) and extracted with dichloromethane (3x50 cm^3). Combined organic phases were washed additionally with water (3x50 cm^3) and dried over MgSO$_4$. The solvent was removed under reduced pressure and the residue was purified by column chromatography (hexane:chloroform 6:1 v/v for **7c** and 2:1 v/v for **9c**).

9-dodecyl-3-iodo-6-(thiophen-2yl)-9H-carbazol (7c): From **6c** 5.87 g (10.0 mmol), yield 1.36 g (25%), slightly yellow solid; ^{1}H NMR (300 MHz, CDCl$_3$) δ: 0.87 (t, $^3J = 6.7$ Hz, 3H, -CH$_3$), 1.10-1.40 (m, 18H), 1.75-1.87 (m, 2H), 4.23 (t, $^3J = 7.2$ Hz, 2H, -CH$_2$-N), 7.10 (dd, $^3J = 5.1$ Hz, $^3J = 3.6$ Hz, 1H, Ti-C$_4$-H), 7.17 (d, $^3J = 8.6$ Hz, 1H, C$_1$-H), 7.26 (dd, $^3J = 5.1$ Hz, $^3J = 1.2$ Hz, 1H, Ti-C$_5$-H), 7.32 (dd, $^3J = 3.6$ Hz, $^4J = 1.2$ Hz, 1H, Ti-C$_3$-H), 7.36 (d, $^3J = 8.6$ Hz, 1H, C$_8$-H), 7.70 (dd, $^3J = 8.6$ Hz, $^4J = 1.7$ Hz, 1H, C$_7$-H), 7.73 (dd, $^3J = 8.6$ Hz, $^4J = 1.7$ Hz, 1H, C$_2$-H), 8.23 (d, $^4J = 1.7$ Hz, 1H, C$_5$-H), 8.42 (d, $^4J = 1.7$ Hz, 1H, C$_4$-H); ^{13}C-NMR (75 MHz, CDCl$_3$) δ: 14.3 (-CH$_3$), 22.8, 27.4, 29.0, 29.5, 29.5, 29.6, 29.7, 29.7 (2xC), 32.0, 43.4 (CH$_2$-N), 81.6 (C$_3$-I), 109.3 (C$_8$), 111.0 (C$_1$), 118.1, 122.2, 122.3, 124.0, 125.1, 125.4, 126.4, 128.1 (C$_7$), 129.5, 134.3, 140.1, 140.2, 145.6 (Ti-C$_2$).

9-dodecyl-3-nitro-6-(thiophen-2yl)-9H-carbazol (9c): From **8c** 5.06 g (10.0 mmol), yield 2.77 g (60%), yellow solid; ^{1}H NMR (300 MHz, CDCl$_3$) δ: 0.87 (t, $^3J = 6.7$ Hz, 3H, -CH$_3$), 1.14-1.45 (m, 18H), 1.82-1.95 (m, 2H), 4.32 (t, $^3J = 7.2$ Hz, 2H, -CH$_2$-N), 7.13 (dd, $^3J = 5.1$ Hz,

^3J = 3.6 Hz, 1H, Ti-C$_4$-H), 7.30 (dd, ^3J = 5.1 Hz, ^3J = 1.2 Hz, 1H, Ti-C$_5$-H), 7.36 (dd, ^3J = 3.6 Hz, ^4J = 1.2 Hz, 1H, Ti-C$_3$-H), 7.38 (d, ^3J = 8.6 Hz, 1H, C$_8$-H), 7.43(d, ^3J = 8.9 Hz, 1H, C$_1$-H), 7.80 (dd, ^3J = 8.6 Hz, ^4J = 1.8 Hz, 1H, C$_7$-H), 8.32 (d, ^4J = 1.8 Hz, 1H, C$_5$-H), 8.37 (dd, ^3J = 8.9 Hz, ^4J = 2.2 Hz, 1H, C$_2$-H), 9.01 (d, ^4J = 2.2 Hz, 1H, C$_4$-H); ^{13}C-NMR (75 MHz, CDCl$_3$) δ: 14.3 (-CH$_3$), 22.8, 27.4, 29.0, 29.5, 29.5, 29.6, 29.7, 29.7 (2xC), 32.0, 43.4 (CH$_2$-N), 81.6 (C$_3$-I), 109.3 (C$_8$), 111.0 (C$_1$), 118.1, 122.2, 122.3, 124.0, 125.1, 125.4, 126.4, 128.1 (C$_7$), 129.5, 134.3, 140.1, 140.2, 145.6 (Ti-C$_2$).

1.8. Synthesis of *3-amino-9-dodecyl-6-(thiophen-2-yl)-9H-carbazoles (10c):*

Compound **10c** was obtained by the same procedure as **5**. From **9c** 2.30 g (5.0 mmol), Pd/C (10%) 0.01 g, N$_2$H$_4$•H$_2$O 5cm^3, 200 cm^3 of EtOH, yield 2.06 g (95%), white solid; ^{1}H NMR (300 MHz, CDCl$_3$) δ: 0.87 (t, ^3J = 6.7 Hz, 3H, -CH$_3$), 1.15-1.42 (m, 18H), 1.75-1.90 (m, 2H), 3.63 (br. s, 2H, -NH$_2$), 4.21 (t, ^3J = 7.2 Hz, 2H, -CH$_2$-N), 6.91 (dd, ^3J = 8.6 Hz, ^4J = 2.3 Hz, 1H, C$_2$-H), 7.09 (dd, ^3J = 5.1 Hz, ^3J = 3.6 Hz, 1H, Ti-C$_4$-H), 7.19-7.26 (m, 2H), 7.28-7.33 (m, 2H), 7.45 (d, ^4J = 2.3 Hz, 1H, C$_4$-H), 7.67 (dd, ^3J = 8.6 Hz, ^4J = 1.8 Hz, 1H, C$_1$-H), 8.20 (d, ^4J = 1.8 Hz, 1H, C$_5$-H); ^{13}C-NMR (75 MHz, CDCl$_3$) δ: 14.2 (-CH$_3$), 22.8, 27.4, 29.2, 29.5, 29.6, 29.6, 29.7, 29.7 (2xC), 32.0, 43.4 (CH$_2$-N), 106.4, 109.0, 109.6, 116.0, 118.1, 121.9, 122.9, 123.5, 123.7, 124.3, 125.0, 128.0, 135.7, 139.3, 140.6, 146.2.

1.9. Buchwald-Hartwig cross-coupling – general procedure for main products

To the mixture of amine **5** or **10** (2.0 mmol), iodo-derivative respectively **3** or **7** (4.5 mmol), and sodium *tert*-butoxide (1.12 g, 10.0 mmol) in dry degassed benzene (30 cm^3) were added tris(dibenzylideneacetone)dipalladium(0) (0.10 g, 0.11 mmol) and tri-*tert*-butylphosphine tetrafluoroborate (0.03 g, 0.11 mmol). The reaction mixture was heated in an argon atmosphere at reflux for 12 h. After cooling, the reaction mixture was diluted with ethyl acetate and the solution was washed with water and brine. Then the organic layer was dried over MgSO$_4$ and filtered. The solvent was removed under reduced pressure and the residue was purified by

column chromatography on silica gel neutralized by triethylamine using hexane:EtOAc:TEA (20:0.8:0.2, v/v) as an eluent.

Tri(9-butyl-9H-carbazol-3-yl)amine (TCA_C4): From **5a** 0.48 g (2.0 mmol), **3a** 1.48 g (4.5 mmol), yield 0.39 g (29%), yellow solid; ^{1}H NMR (300 MHz, DMSO-d_6) δ: 0.90 (t, ^3J = 7.3 Hz, 9H, -CH$_3$), 1.27-1.41 (m, 6H, -CH$_2$-CH$_3$), 1.68-1.82 (m, 6H, -CH$_2$-CH$_2$CH$_3$), 4.35 (t, ^3J = 6.5 Hz, 6H, -CH$_2$-N), 7.02 (t, ^3J = 7.5 Hz, 3H, C$_6$-H), 7.22 (dd, ^3J = 8.7 Hz, ^4J = 2.2 Hz, 3H, C$_2$-H), 7.38 (ddd, ^3J = 8.3 Hz, ^3J = 7.5 Hz, ^4J = 1.2 Hz, 3H, C$_7$-H), 7.50 (d, ^3J = 8.7 Hz, 3H, C$_1$-H), 7.55 (d, ^3J = 8.3 Hz, 3H, C$_8$-H), 7.83 (d, ^4J = 2.2 Hz, 3H, C$_4$-H), 7.89 (d, ^3J = 7.5 Hz, 3H, C$_5$-H); ^{13}C-NMR (75 MHz, DMSO-d_6) δ: 13.7 (3x-CH$_3$), 19.8 (3x-CH$_2$-CH$_3$), 30.8 (3x-CH$_2$-CH$_2$CH$_3$), 42.1 (3x-CH$_2$-N), 109.1, 110.0, 115.1, 118.2, 120.3, 121.7, 122.8, 123.3, 125.6, 130.0, 140.5, 141.9. Anal. Calc. for C$_{48}$H$_{48}$N$_4$: C, 84.67; H, 7.11; N, 8.23. Found: C, 84.71; H, 7.13; N, 8.16.

Tri(9-octyl-9H-carbazol-3-yl)amine (TCA_C8): From **5b** 0.59 g (2.0 mmol), **3b** 1.83 g (4.5 mmol), yield 0.52 g (31%), yellow solid; ^{1}H NMR (300 MHz, DMSO-d_6) δ: 0.80 (t, ^3J = 6.3 Hz, 9H, -CH$_3$), 1.10-1.40 (m, 30H), 1.67-1.85 (m, 6H), 4.34 (t, ^3J = 6.5 Hz, 6H, -CH$_2$-N), 7.03 (t, ^3J = 7.5 Hz, 3H, C$_6$-H), 7.22 (dd, ^3J = 8.6 Hz, ^4J = 2.1 Hz, 3H, C$_2$-H), 7.38 (ddd, ^3J = 8.3 Hz, ^3J = 7.5 Hz, ^4J = 1.2 Hz, 3H, C$_7$-H), 7.48-7.56 (m, 6H, C$_1$-H and C$_8$-H), 7.81 (d, ^4J = 2.1 Hz, 3H, C$_4$-H), 7.89 (d, ^3J = 7.5 Hz, 3H, C$_5$-H). Anal. Calc. for C$_{60}$H$_{72}$N$_4$: C, 84.86; H, 8.55; N, 6.60.

Tri[9-dodecyl-6-(thiophen-2-yl)-9H-carbazol-3-yl]amine (ThTCA_C12): From **10c** 0.86 g (2.0 mmol), **7c** 2.44 g (4.5 mmol), yield 0.61 g (24%), yellow-green solid; ^{1}H NMR (300 MHz, CDCl$_3$) δ: 0.86 (t, ^3J = 6.5 Hz, 9H, -CH$_3$), 1.17-1.40 (m, 54H), 1.82-1.97 (m, 6H), 4.27 (t, ^3J = 7.0 Hz, 6H, -CH$_2$-N), 7.00 (dd, ^3J = 5.1 Hz, ^4J = 3.6 Hz, 3H, Ti-C$_4$-H), 7.15 (dd, ^3J = 5.1 Hz, ^4J = 1.0 Hz, 3H, Ti-C$_5$-H), 7.24 (dd, ^3J = 3.6 Hz, ^4J = 1.0 Hz, 3H, Ti-C$_3$-H), 7.30-7.40 (m, 9H), 7.67 (dd, ^3J = 8.5 Hz, ^4J = 1.8 Hz, 3H), 7.93 (d, ^4J = 1.8 Hz, 3H, C$_4$-H), 8.12 (d, ^3J = 1.8 Hz,

3H, C_5-H); ^{13}C-NMR (75 MHz, CDCl$_3$) δ: 14.0 (3x-CH$_3$), 22.5, 27.2, 29.0, 29.2, 29.3, 29.4, 29.5, 31.8, 43.2 (3x-CH$_2$-N), 108.9, 109.5, 115.7, 117.9, 121.7, 122.9, 123.2, 123.4, 123.8, 124.1, 125.2, 127.8, 136.9, 140.4, 142.4, 145.6. Anal. Calc. for C$_{84}$H$_{102}$N$_4$S$_3$: C, 79.82; H, 8.13; N, 4.43.

2. ^{1}H and ^{13}C-NMR spectra
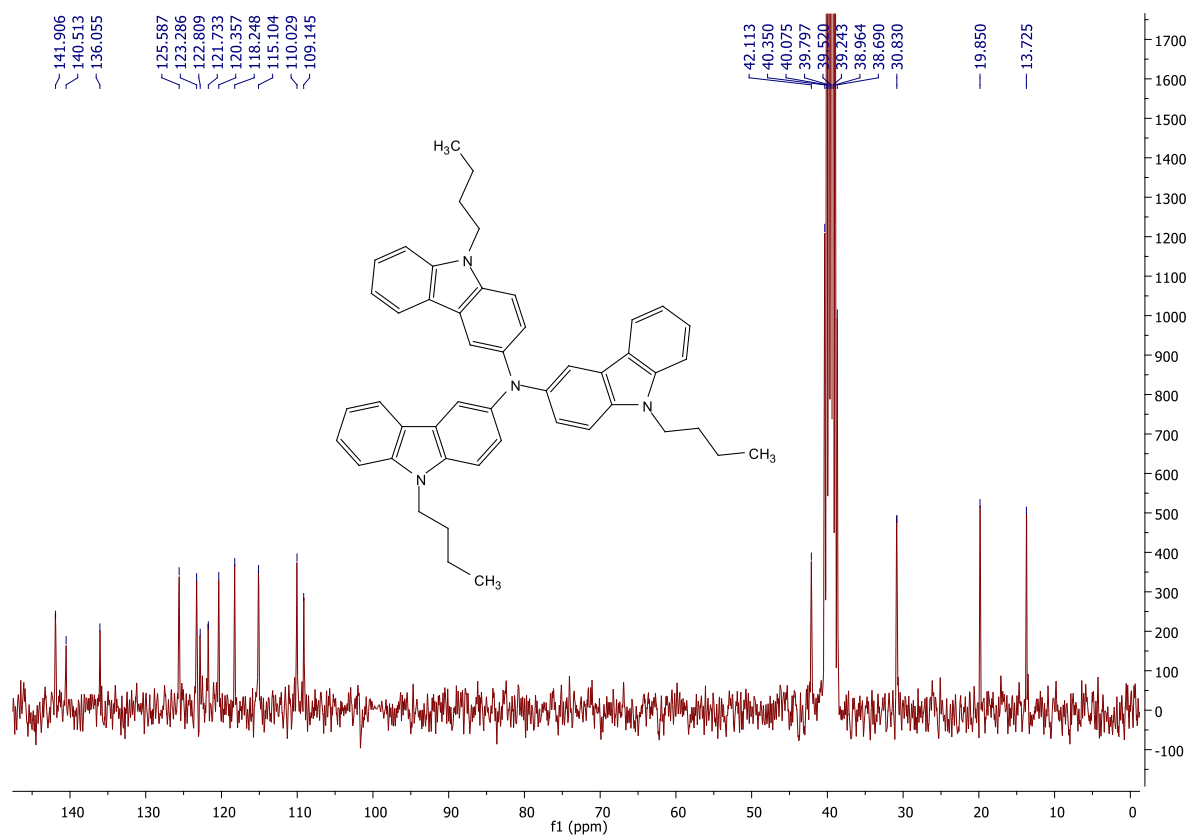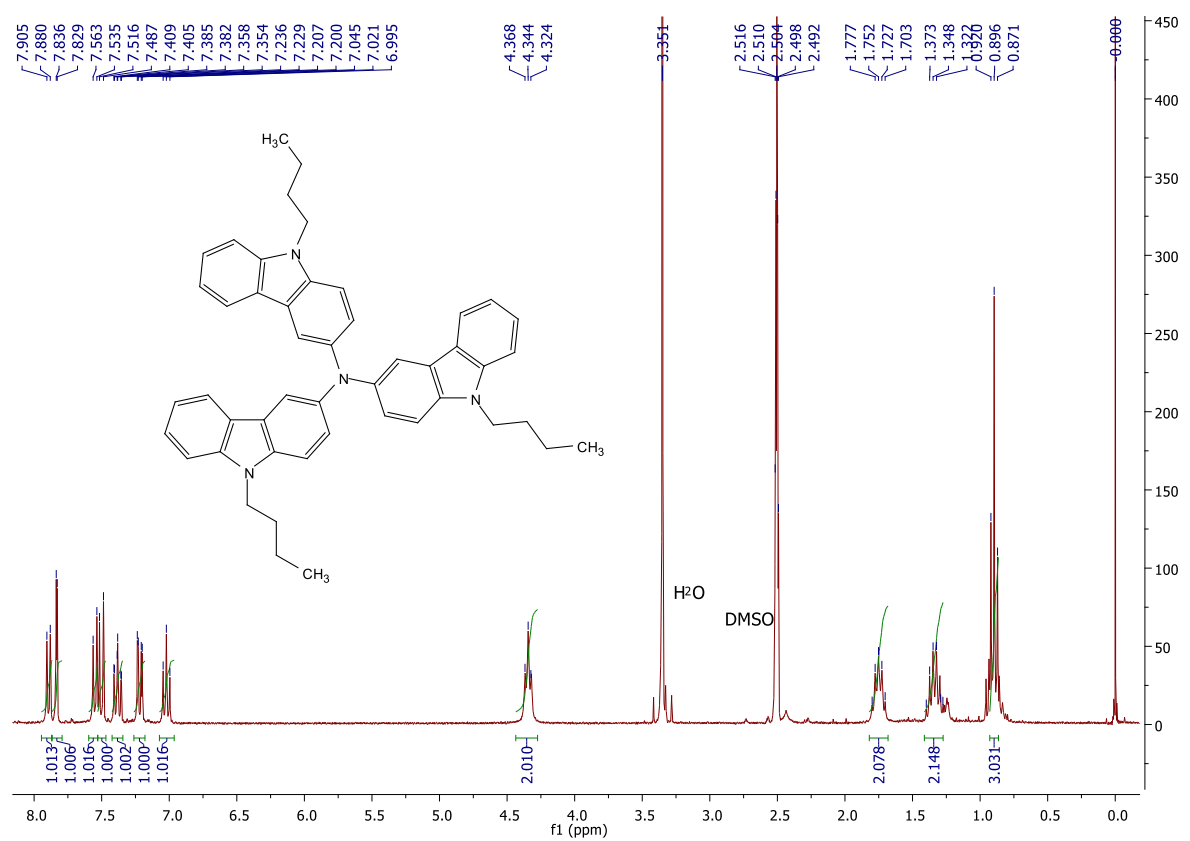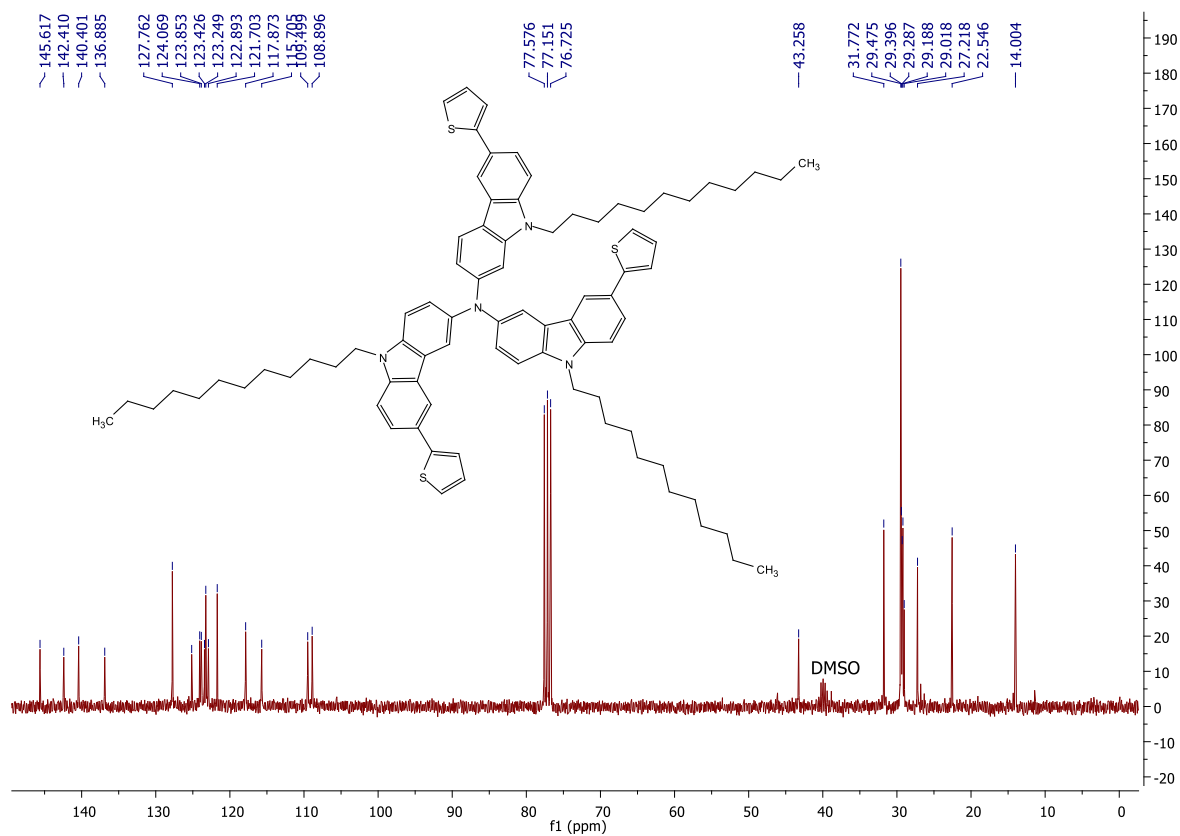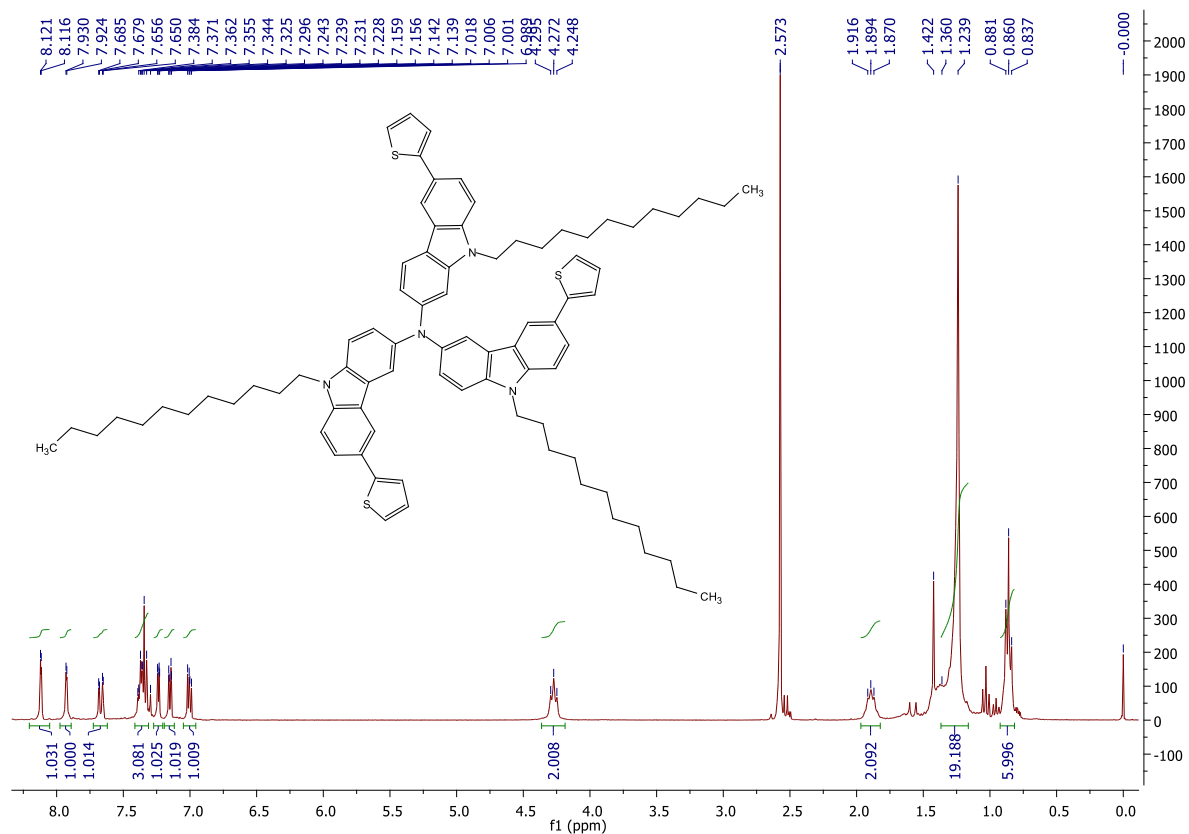
3. Experimental

3.1 Photoluminescence

Zeonex ® 480 blends were prepared from toluene solutions by the drop-cast method and dried at 90 ˚C, mCP films were co-deposited using the same method as in OLED fabrication (see below). All solutions were investigated at 10^{-5} mol dm^{-3} concentration. Absorption and emission spectra were collected using a UV-3600 double beam spectrophotometer (Shimadzu), and a Fluoromax fluorescence spectrometer (Jobin Yvon).

Phosphorescence, prompt fluorescence (PF), and delayed fluorescence (DF) spectra and decays were recorded using nanosecond gated luminescence and lifetime measurements (from 400 ps to 1 s) using either third harmonics of a high-energy, pulsed Nd:YAG laser emitting at 355 nm (EKSPLA) or a N$_2$ laser emitting at 337 nm. Emission was focused onto a spectrograph and detected on a sensitive gated iCCD camera (Stanford Computer Optics) of sub-nanosecond resolution. PF/DF time-resolved measurements were performed by exponentially increasing gate and delay times.

3.2 OLED fabrication and characterization

All organic evaporated compounds were purified by a Creaphys organic sublimation system, mCP - 1,3-Bis(carbazol-9-yl)benzene (TCI-Europe), NPB - *N,N′*-Di-1-naphthyl-*N,N′*-diphenylbenzidine (TCI-Europe), TPBi - 2,2',2"-(1,3,5-Benzinetriyl)-tris(1-phenyl-1-H-benzimidazole) (LUMTEC), TCTA - 4,4',4"-Tris(carbazol-9-yl)triphenylamine (TCI-Europe), CzSi - 9-(4-tert-butylphenyl)-3,6-bis(triphenylsilyl)-9H-carbazole (LUMTEC), TCBPA - (LUMTEC), LiF (99.995%, Sigma Aldrich), Aluminium wire (99.9995%, Alfa Aesar). OLED devices were fabricated using pre-cleaned indium-tin-oxide (ITO) coated glass substrates with a sheet resistance of 20 Ω/cm^2 and ITO thickness of 100 nm. The OLED devices had a pixel size of 4 mm by 2 mm. All organic and cathode layers were thermally evaporated using Kurt J.

Lesker Spectros II deposition at 10^{-6} mbar. All organic materials and aluminium were deposited at a rate of 1 Å s^{-1} and between 0.1 – 2 Å s^{-1} for coevaporated layers. The LiF layer was deposited at 0.2 Å s^{-1}. Characterisation of OLED devices was conducted in 10 inch integrating sphere (Labsphere) connected to a Source Measure Unit.

3.2 Quasi-CW PIA measurements

Measurement of the excited-state absorption (and emission) spectra, were performed using a 375 nm pump beam (Vortran Stradus 375–60) modulated at 73 Hz, with a continuous laser-driven white light source (Energetiq EQ-99X) as the probe. The probe beam was then passed through a Bentham TM300 monochromator and incident on a Si detector connected to the Signal Recovery dual channel 7,225 digital lock-in amplifier that also provides the reference frequency modulation for the pump laser.

3.3 Calculations

For clarity, the calculation details are explained in the sections preceding the respective results.

4. Additional results for TCA_C4
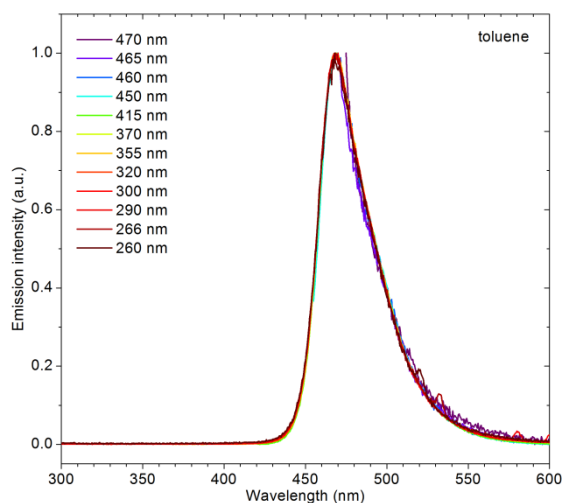
Figure S1. Photoluminescence of **TCA_C4** in toluene as a function of excitation wavelength.

The emission profile of **TCA_C4** shows no contribution of any upper excited state emission, such as local etc. due to being independent of excited absorption band (excitation wavelength). As such the photoluminescence is always generated from the lowest singlet state.

Table S1. Extinction coefficients ($M^{-1} cm^{-1}$) of **TCA_C4** in MCH.

λ_{max}, nm	413 nm	376 nm	321 nm	290 nm
ε, $M^{-1} cm^{-1}$	3900	8300	75800	63000
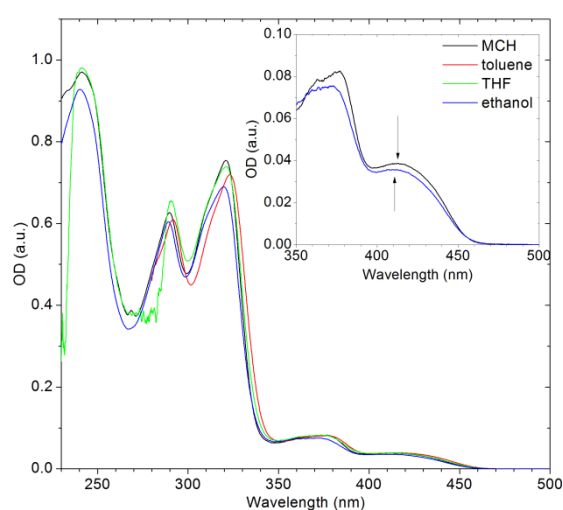
Figure S2. Absorption spectra of **TCA_C4** in solvents of different polarity. Please note a visible change is observed between MCH and ethanol suggesting that the two lowest absorption bands have some n-π* character. A small blue shift in more polar ethanol is observed.

Table S2. Photoluminescence quantum yields and degassing ratios for **TCA_C4**.

	Φ_{PL} (air)	Φ_{PL} (degassed)	Degassing factor	DF/PF ratio (%DF)
Toluene	0.25	0.62	2.43	-
mCP (10%)	0.71	0.86	1.21	0.45 (31%)
zeonex (1%)	0.70	0.89	1.27	0.43 (30%)

It is worth to note that Φ_{PL} values of **TCA_C4** in solid film and solution are related to each other. Degassed solution shows nearly 70% the value of Φ_{PL} in degassed solid samples which is equal the contribution of PF in solid films as determined from the time-resolved decay. Note Φ_{PL} of non-degassed (in air) films is slightly higher than degassed solution suggesting some TADF is still present. This is possible because O_2 diffusion through solid films is relatively slow and significantly slower than in solutions.
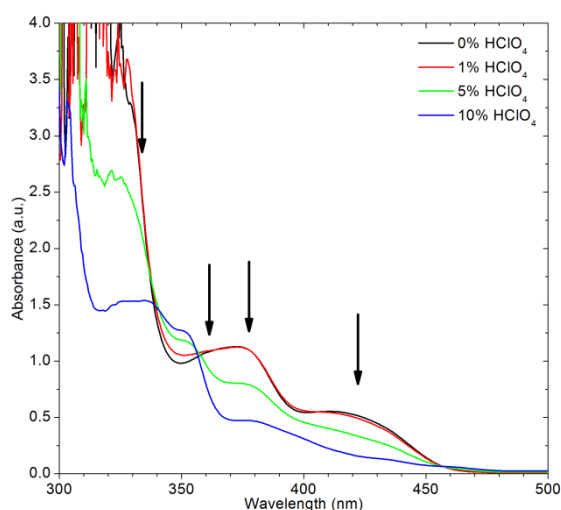
Figure S3. UV-Vis spectrophotometric titration of **TCA_C4** in THF with $HClO_4$.

To further prove the n-π^* character of the lowest energy absorption bands the **TCA_C4** molecule was titrated with concentrated $HClO_4$ (**Figure S3**). Bands affected by protonation should in principle decrease their intensity. This happens to, among others, the two lowest absorption bands, which is in agreement with other observations suggesting their n-π^* character.
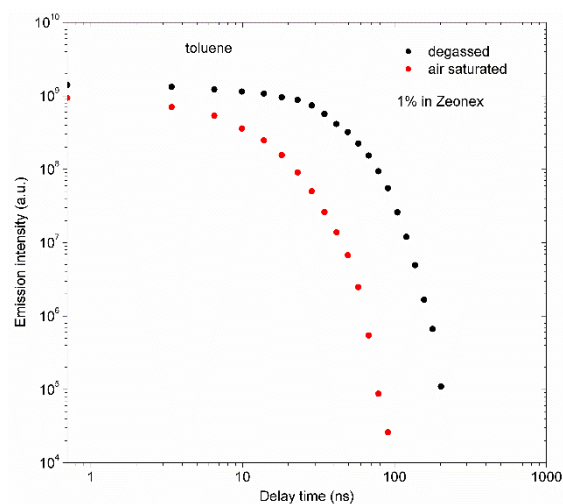
Figure S4. Time-resolved photoluminescence decay of **TCA_C4** in air-equilibrated and degassed toluene recorded with the gated iCCD camera. Note no long-lived components are observed.
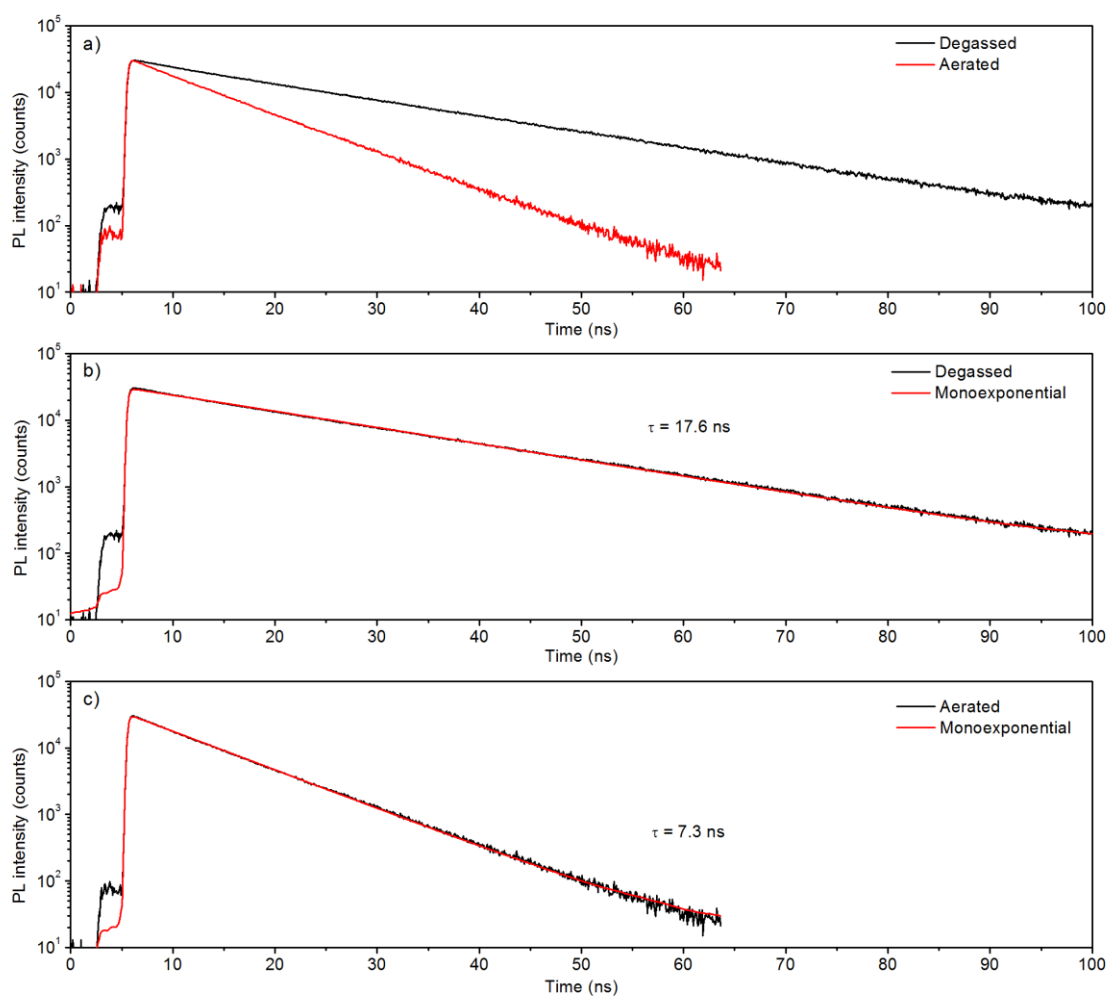
Figure S5. Time-resolved photoluminescence decay of **TCA_C4** in air-equilibrated and degassed toluene recorded with TCSPC using 405 nm diode laser excitation.
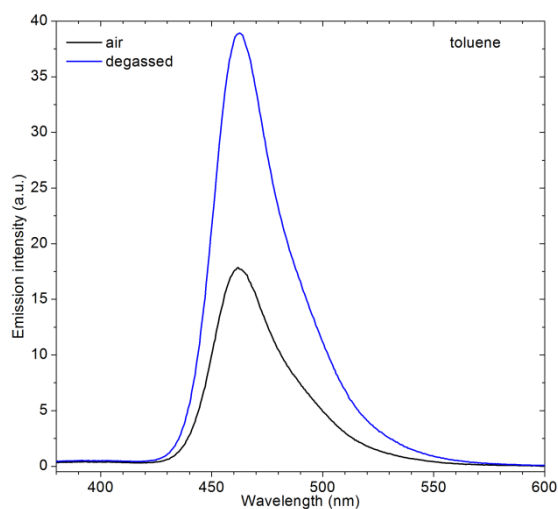
Figure S6. Steady-state photoluminescence spectrum (λ_{exc} = 355 nm) of **TCA_C4** in air-equilibrated and degassed toluene recorded with a fluorometer.
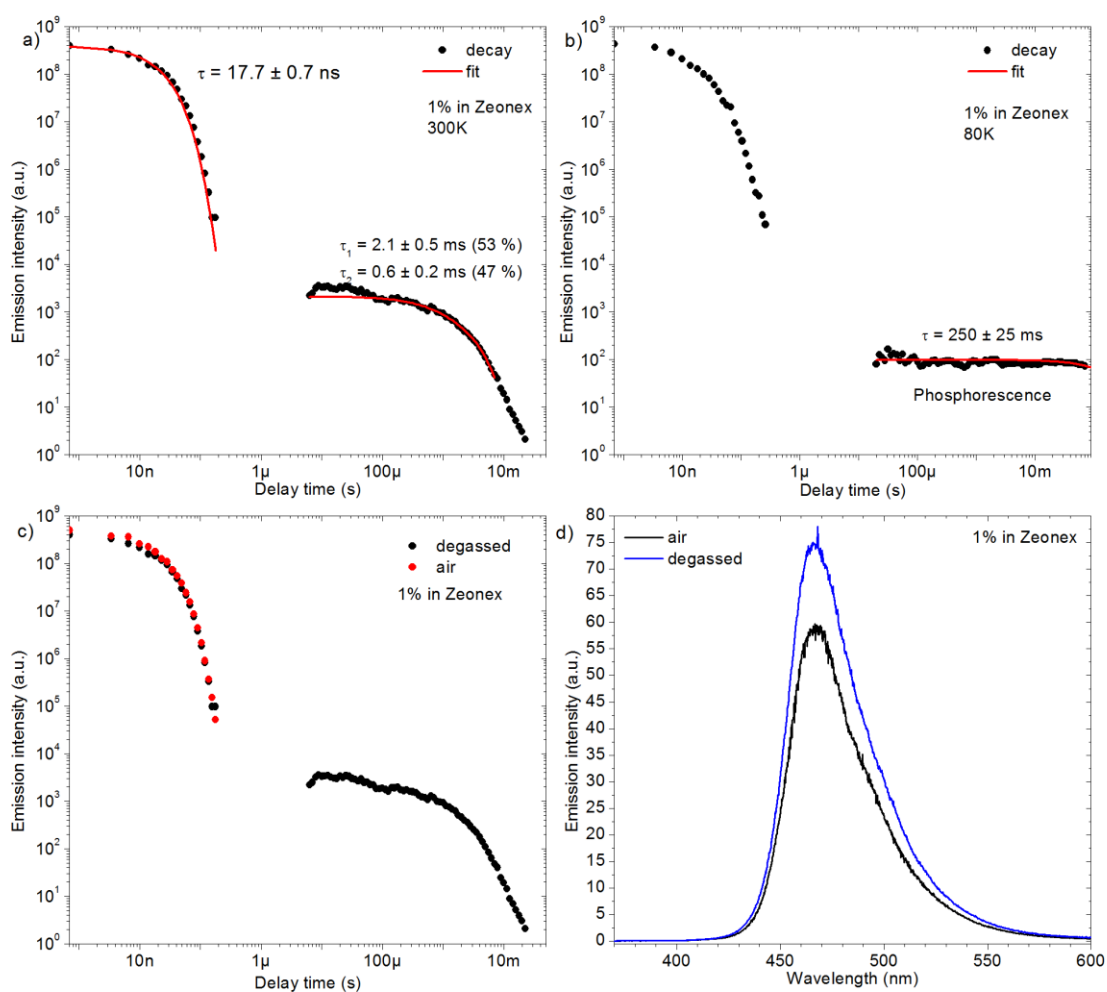
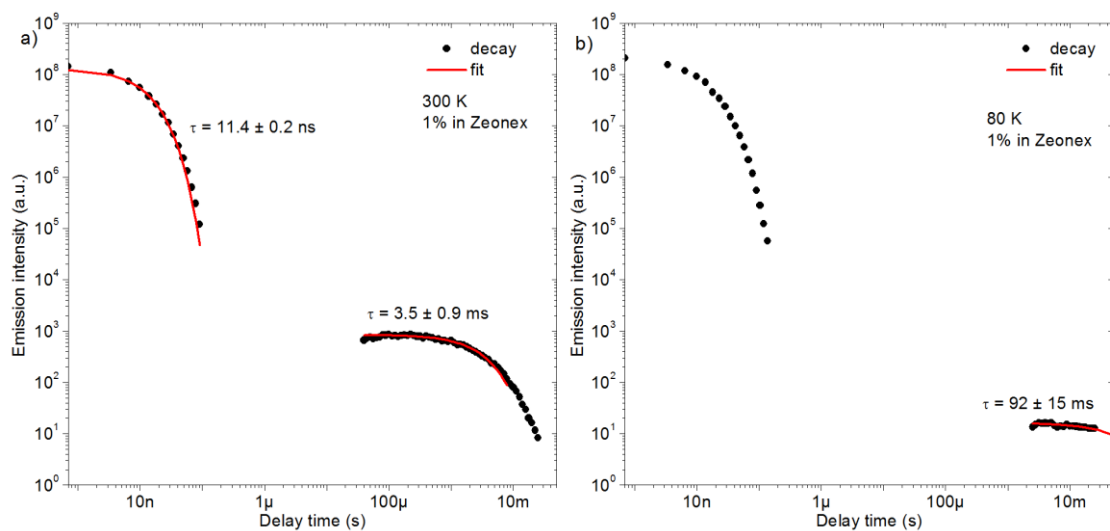**Figure S7.** Time-resolved and steady-state photoluminescence study of **TCA_C4** in zeonex. a) Room temperature decay with time constants; b) low-temperature decay with time

constants; c) room temperature decay in air and vacuum; d) steady-state spectra in air and
vacuum.
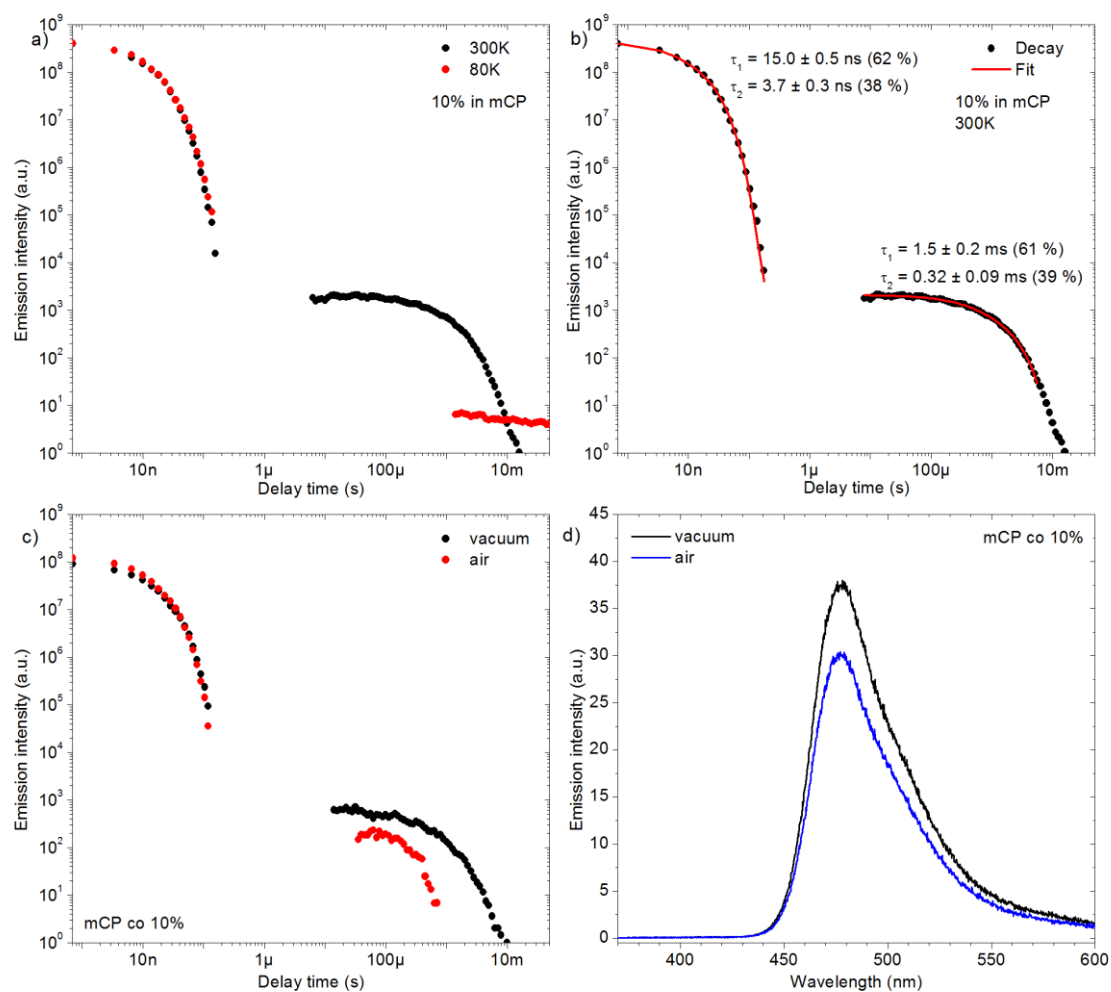
Figure S8. Time-resolved and steady-state photoluminescence study of **TCA_C4** in mCP. a)
Room and low-temperature decay; b) room temperature decay with time constants; c) room
temperature decay in air and vacuum; d) steady-state spectra in air and vacuum.
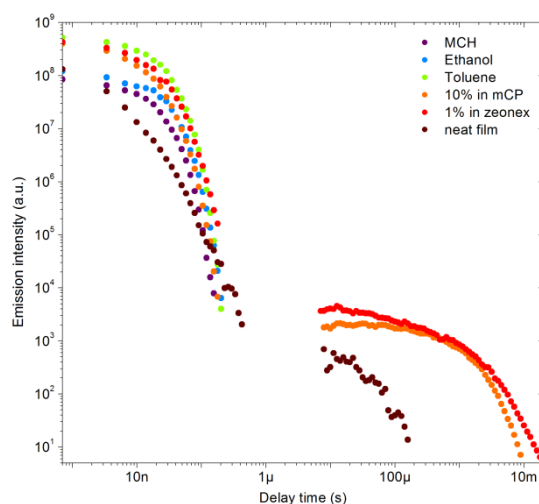
Figure S9. Photoluminescence decay in different environments at room temperature in vacuum or degassed solution of **TCA_C4**.

Prompt fluorescence decay is nearly the same regardless of the solvent polarity (**Figure S9**). TADF is quenched in solutions and is only observed in films in a host matrix. In the neat film, concentration quenching and formation of excimeric species can be observed (see **Figure S9** and **S17**) suggesting that the excimeric species quench the excitonic states of **TCA_C4**.
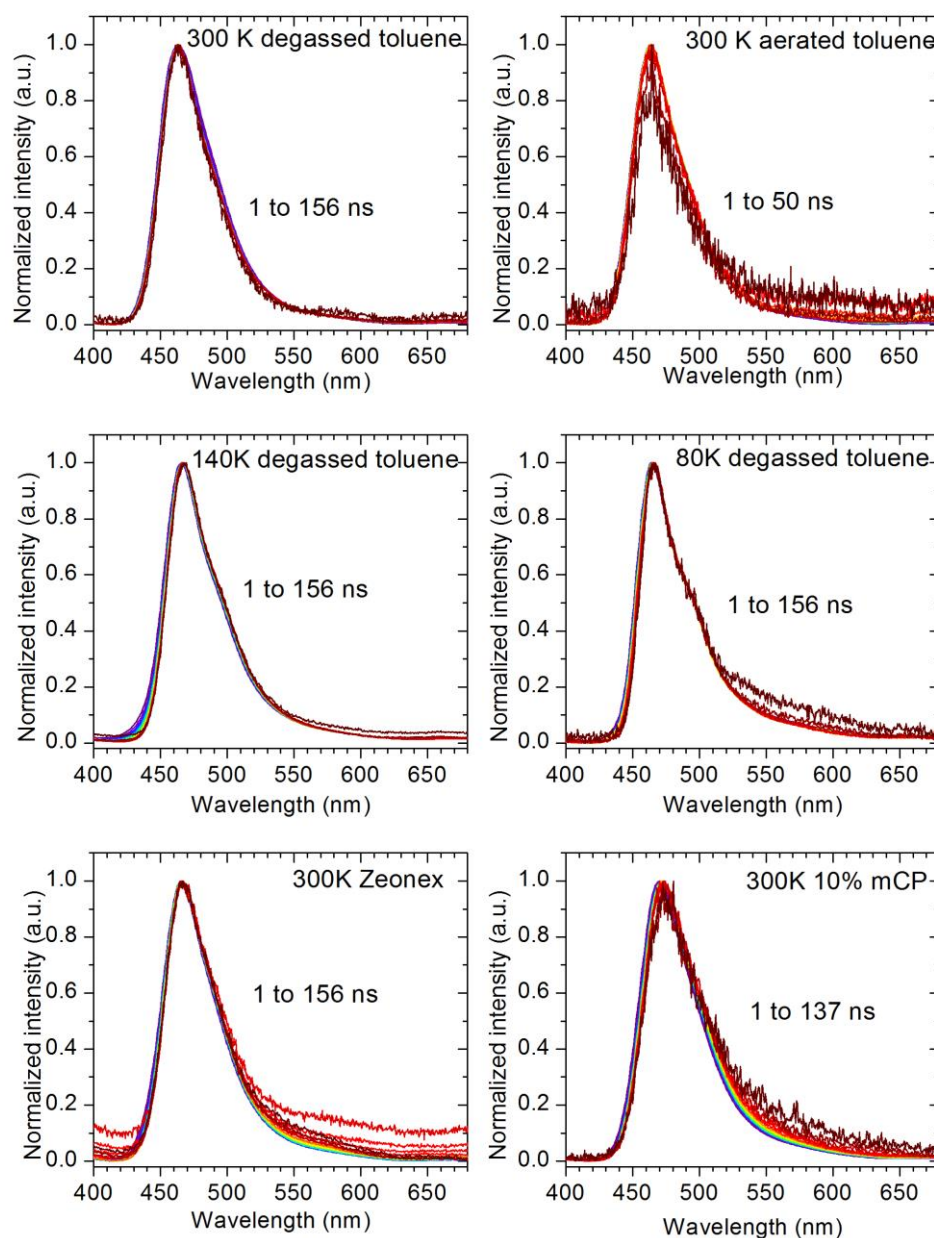
Figure S10. Time-resolved photoluminescence spectra of **TCA_C4** in different environments and temperatures recorded with the iCCD camera using 355 nm laser excitation. Note only spectra of the fast component are shown here.
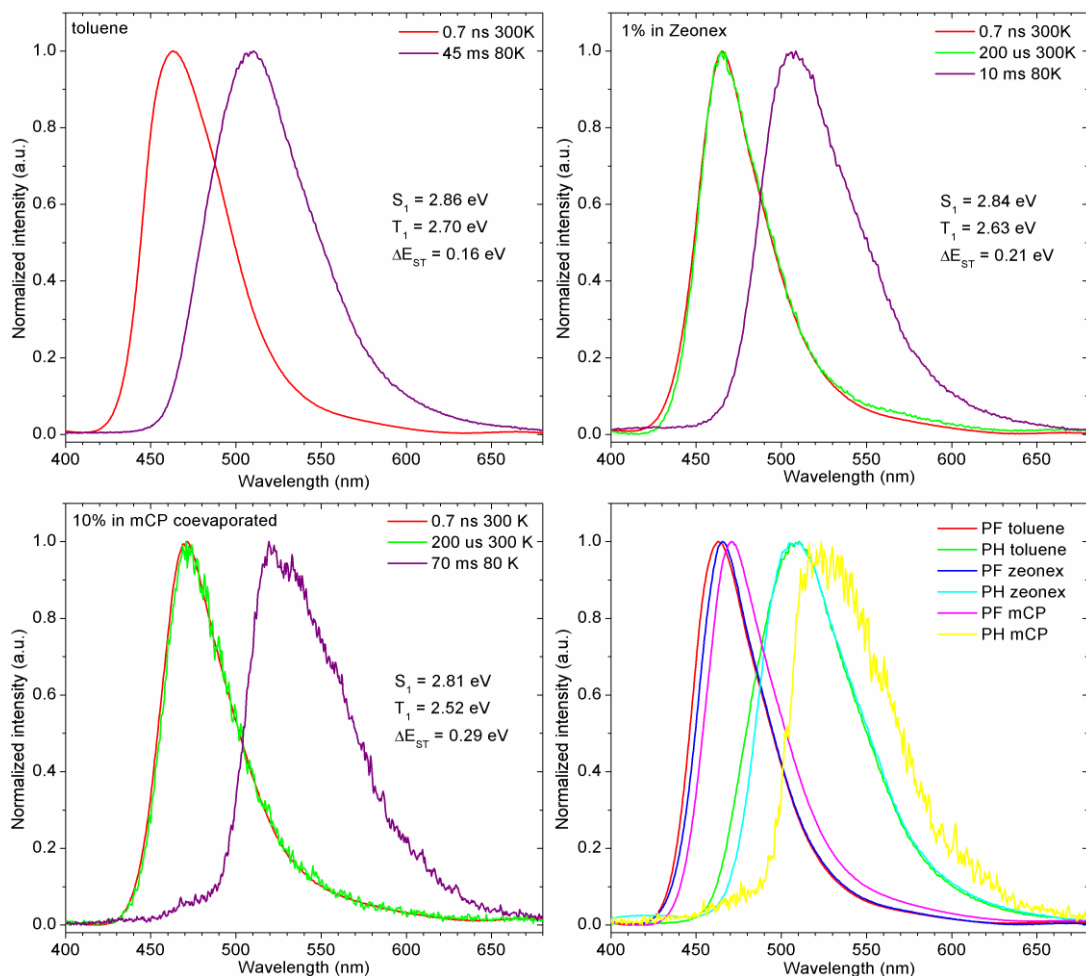
Figure S11. Time-resolved photoluminescence spectra of **TCA_C4** in toluene, zeonex, and mCP.

Fluorescence and phosphorescence do not show any significant vibronic structure (**Figure S11**). Interestingly, the fluorescence of **TCA_C4** shows no significant change in different hosts, but clearly redshifts in mCP compared to toluene. The most interesting is the behaviour of the phosphorescence spectrum as it significantly redshifts in mCP. Molecular packing of the mCP host molecules compresses the **TCA_C4** molecule, disturbing its structural geometry and making it slightly more planar. This causes the spin exchange energy to rise, thus the decrease in singlet energy (S_1), relative to toluene or zeonex, is smaller than the decrease in triplet energy (T_1) which as a result gives a larger E_{S-T} in this host. The rise in E_{S-T} in mCP relative to zeonex (0.29 eV and 0.21 eV, respectively) does not affect the TADF properties, such as DF lifetime. This can be explained as the $S_1 - T_1$ energy difference is not the actual energy barrier for the molecule. In fact the energy barrier is related to the $T_1 - T_2$ energy gap as described in main text. Most likely an effect causing a decrease of T_1 energy should also affect the upper triplets' energy, also decreasing it. Therefore, the T_1 may go along with T_2 and the $T_1 - T_2$ energy gap

may remain unchanged. If the $T_1 - T_2$ gap remains the same as in zeonex, the TADF lifetime is not affected.
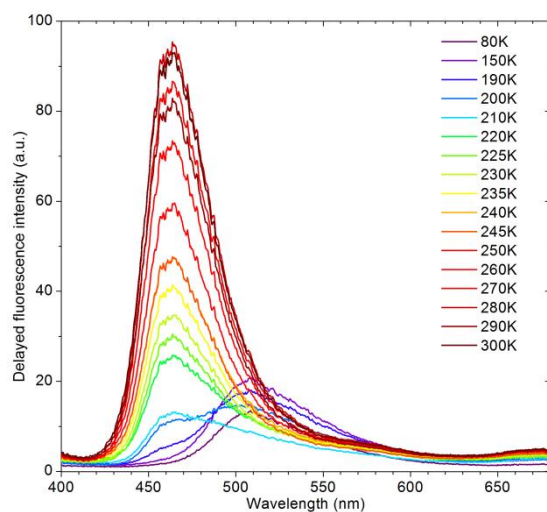
Figure S12. Gated photoluminescence spectra of the TADF component in **TCA_C4** in zeonex at various temperatures.
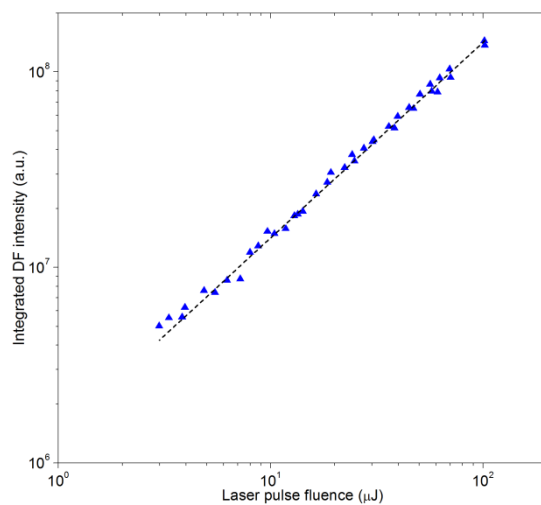
Figure S13. Power dependence of delayed fluorescence of **TCA_C4** in zeonex.
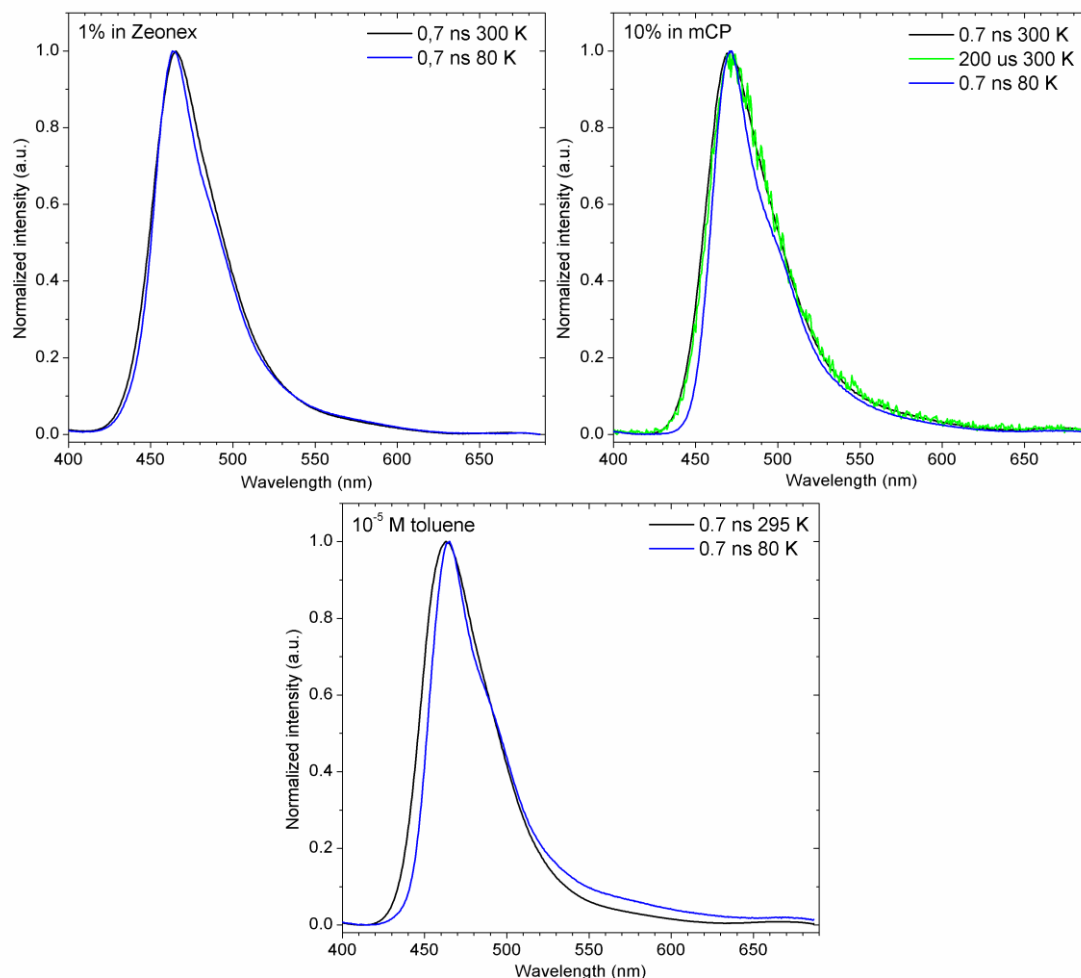
Figure S14. Prompt and delayed fluorescence spectra of **TCA_C4** in various environments.

One can note the prompt fluorescence at 300 K in mCP and also in toluene have a blue edge that disappears at 80 K making the PF visibly red-shifted at 80K compared to the 300 K spectra (**Figure S14**). This shows the emission arising at room temperature originates not only from the ground vibronic level of the S_1 state (as it typically does), but also a contribution from an upper vibronic level is observed. This "hot" emission suggests that the lowest singlet state remains in thermal equilibrium with its vibronic levels at 300 K. Moreover, the prompt and delayed fluorescence at 300 K are identical (including the presence of the blue edge), which again shows the "hot", upper vibronic state emission is observable for miliseconds. This means the associated vibronic state can be accessed regardless of the delay. The effect is not observed in zeonex as there is always free void in the polymer matrix allowing the molecule to structurally relax and presumably vibrationally cool.
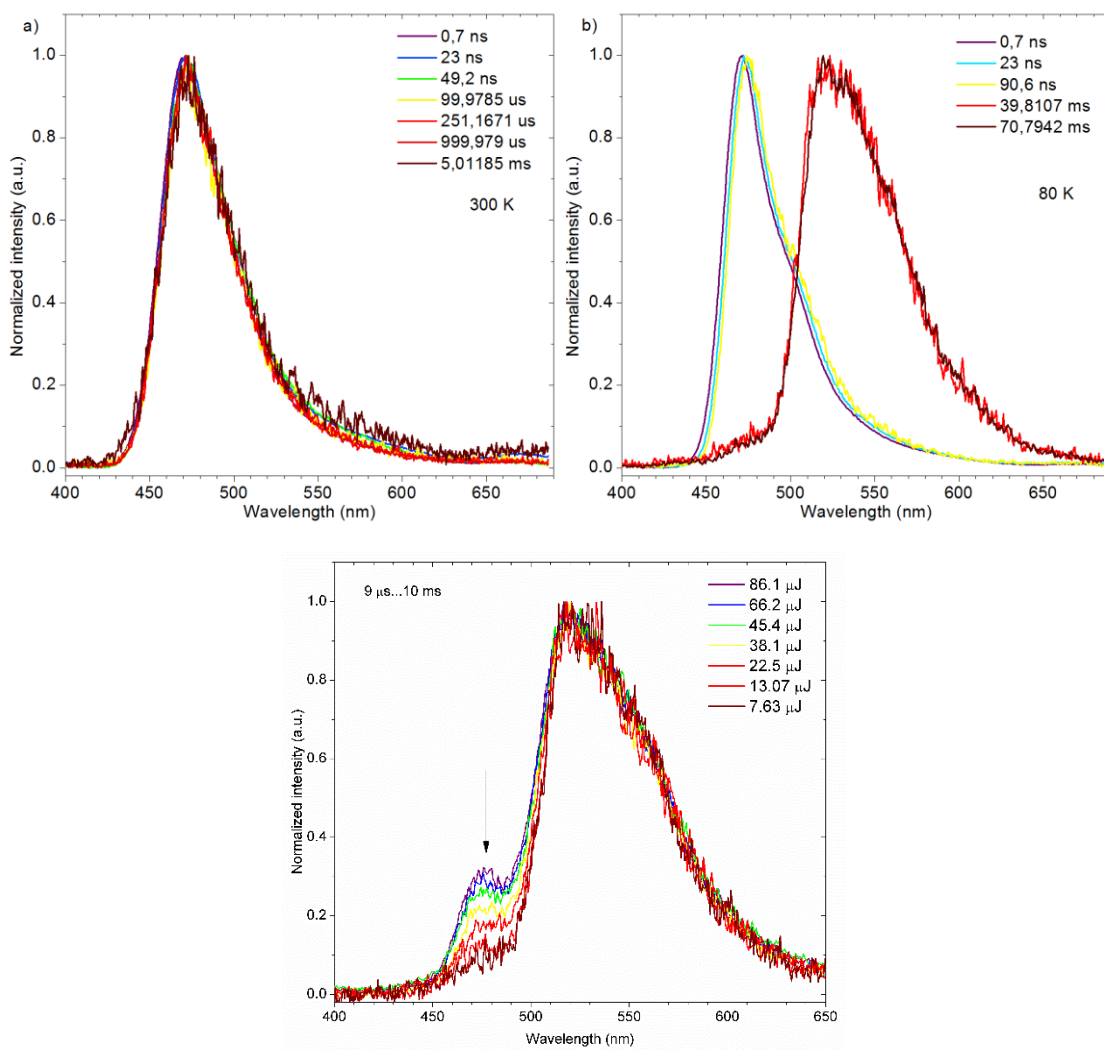
Figure S15. Time-resolved spectra of **TCA_C4** in mCP at different temperatures (top). Phosphorescence spectra recorded at various laser pulse energy at 80 K (bottom).

One can note a foot in the **TCA_C4** phosphorescence spectrum is caused by triplet-triplet annihilation at 80 K as shown in **Figure S15**. The presence of triplet-triplet annihilation is evidenced by its supralinear power dependence resulting in visible existence of delayed fluorescence at higher laser pulse energy and decrease to only a shoulder with no visible peak at low power.
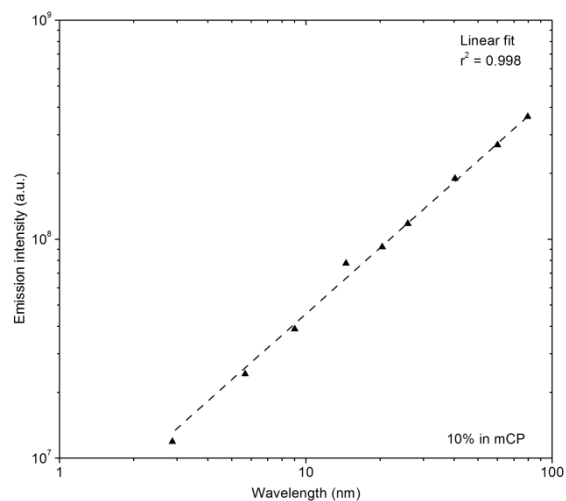
Figure S16. Power dependence of the delayed fluorescence component in **TCA_C4** / mCP blend.
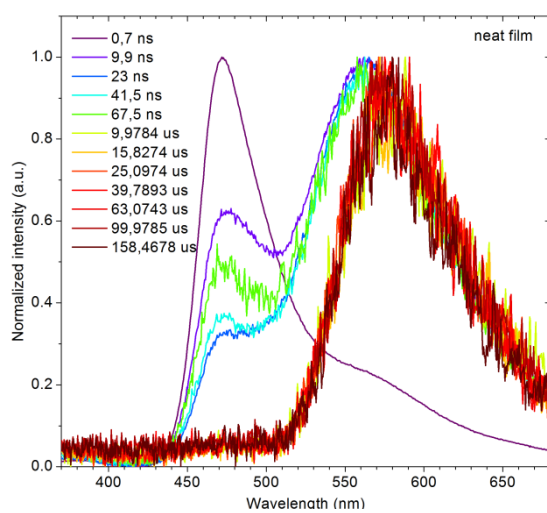
Figure S17. Time-resolved photoluminescence spectra of **TCA_C4** in neat film at room temperature recorded with an iCCD camera using 355 nm laser excitation. Note strong contribution of excimer emission is observed.

5. Results for ThTCA_C12

Table S3. Photoluminescence quantum yield and degassing ratio for **ThTCA_C12**.

	Φ_{PL} (air)	Φ_{PL} (degassed)	Degassing factor
Toluene	0.18	0.31	1.73

Φ_{PL} of **ThTCA_C12** is visibly lower than of **TCA_C4** (see **Table S1**), but also here a large degassing factor is observed. Due to identical electronic properties and similar photophysical behaviour the mechanism governing the prompt fluorescence quenching is believed to be identical in **ThTCA_C12** as in **TCA_C4**.
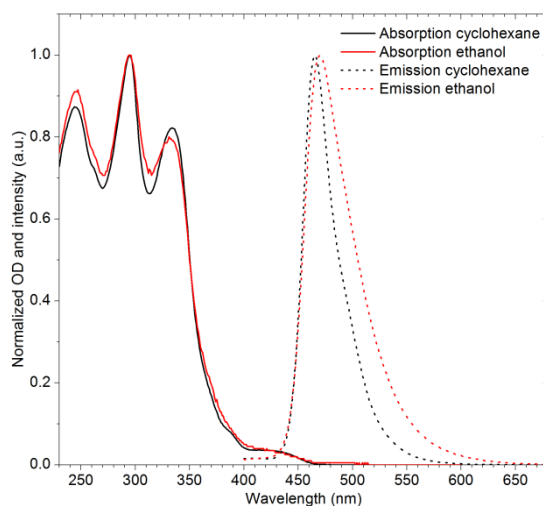
Figure S18. Absorption and fluorescence spectra of **ThTCA_C12** in solvents of different polarity.
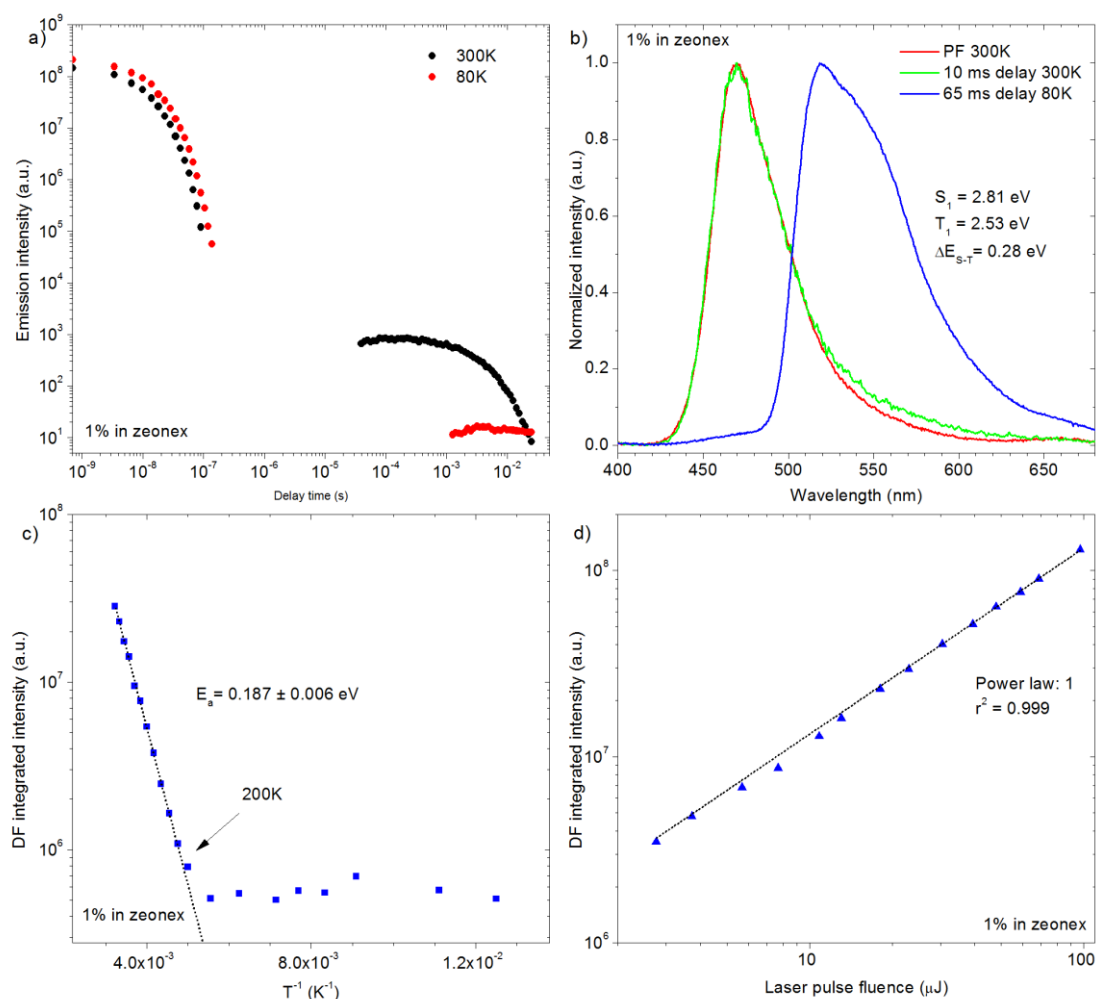
Figure S19. Time-resolved photoluminescence study of **ThTCA_C12** in zeonex at room temperature recorded with an iCCD camera using 355 nm laser excitation. a) Decays at different temperatures; b) Time-resolved spectra; c) DF temperature dependence; d) DF power dependence.

Figure S20. Time-resolved and steady-state photoluminescence study of **ThTCA_C12** in zeonex. a) Room temperature decay with time constants; b) low-temperature decay with time constants.
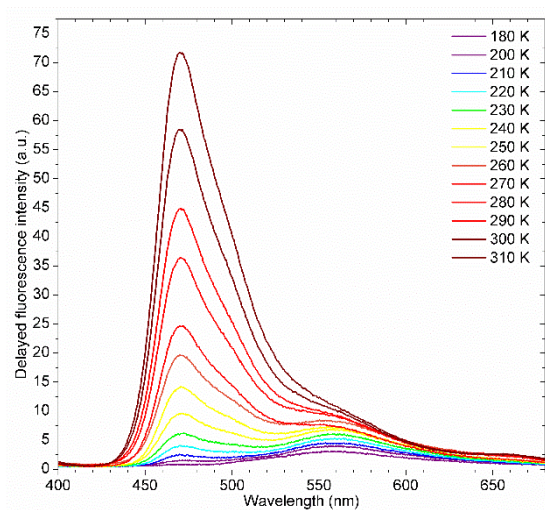
Figure S21. Gated photoluminescence spectra of the delayed fluorescence of **ThTCA_C12** 1% in zeonex as a function of temperature.

6. Results for TCA_C8
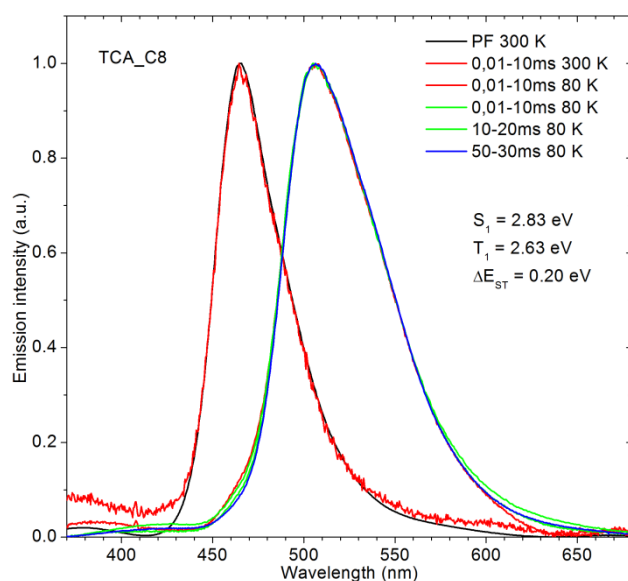
Figure S22. Time-resolved photoluminescence spectra of **TCA_C8** in zeonex at different temperatures recorded with an iCCD camera using 355 nm laser excitation.

TCA_C8, similarly to **TCA_C4**, also shows delayed fluorescence and the same S_1 and T_1 energy, thus we conclude that the alkyl chain does not affect molecule properties and TCA with any *n*-alkyl chain should show the same properties, assuming there is no additional steric hindrance caused by the chain (i.e. branched substituents may change ground state and excited state structural geometry affecting excited state energy levels and the coupling between them).

7. Calculations

DFT/TDDFT calculations were carried out with B3LYP hybrid functional combined with 6-31G(d) basis set, using model molecules with alkyl chains cut to C2 (**TCA** and **ThTCA**). For investigated compounds, ground state geometries were optimized with no symmetry constraints to a local minimum, which was followed by frequency calculations. In all cases, no negative frequencies were found. Excited state geometries (both singlet and triplet) were then calculated using a combination of B3LYP functional and MIDIX[S4,S5] basis set. Due to problems with convergence, for these geometry optimizations, we also typed opt=loose into the input file. Excited states energies were then calculated on obtained geometries with TDDFT/B3LYP/6-31G(d)/PCM(MCH). All calculations in this work were conducted with polarizable continuum model (PCM) using methylcyclohexane (MCH) as solvent as implemented in Gaussian 09 software. Input files and molecular orbital plots were prepared with Gabedit 2.4.7 software.[S6] All calculations had been carried with Gaussian 09 software.[S7]
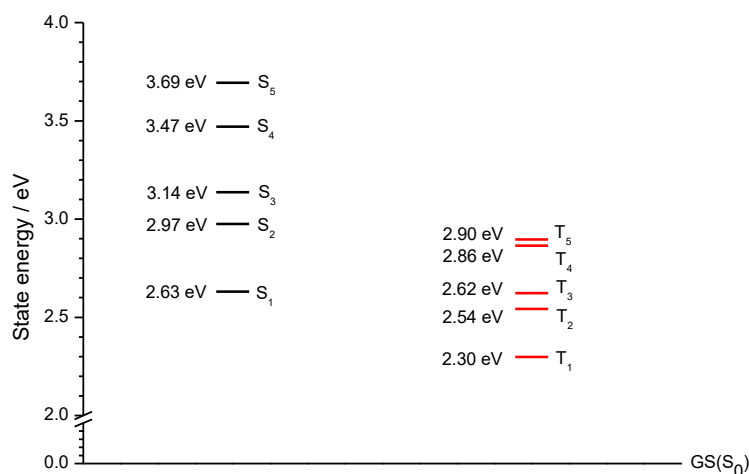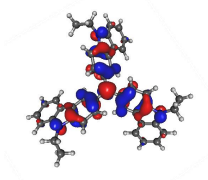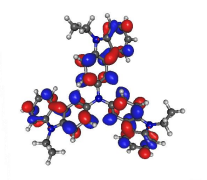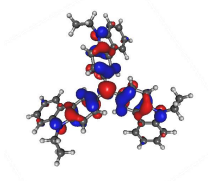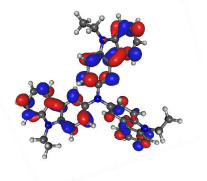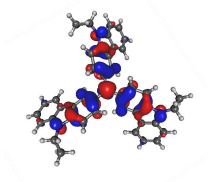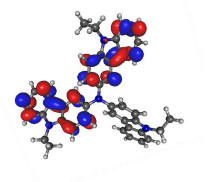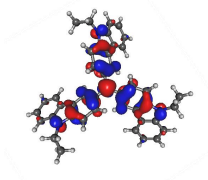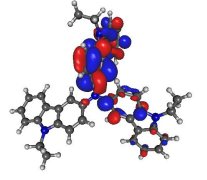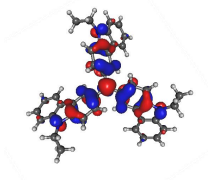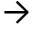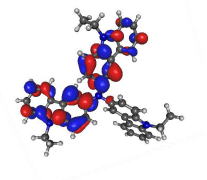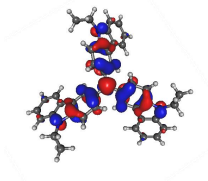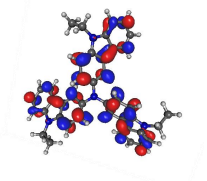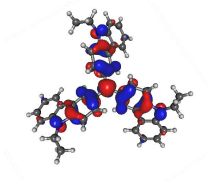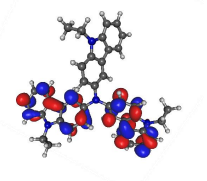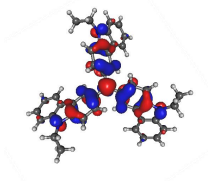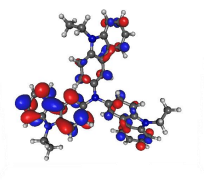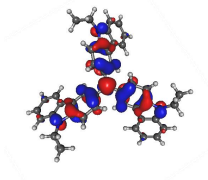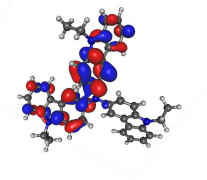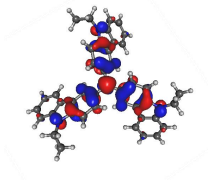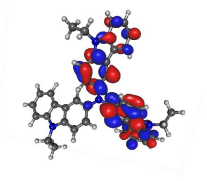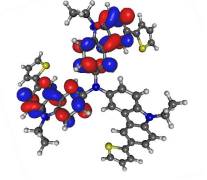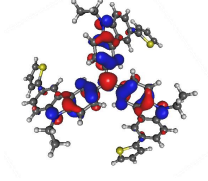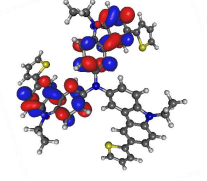

Figure S23. Calculated energy levels of **TCA**.

Table S4. Summary of excited states in **TCA**

State	Transition			State character
S_1	HOMO	→	LUMO	$n\pi^* + \pi\pi^*$
S_2	HOMO	→	LUMO+1	$n\pi^* + \pi\pi^*$
S_3	HOMO	→	LUMO+2	$n\pi^* + \pi\pi^*$
S_4	HOMO	→	LUMO+3	$n\pi^* + \pi\pi^*$
S_5	HOMO	→	LUMO+4	$n\pi^* + \pi\pi^*$
T_1	HOMO	→	LUMO	$n\pi^* + \pi\pi^*$

T$_2$	HOMO	→	LUMO+1	nπ* + $\pi\pi$*
T$_3$	HOMO	→	LUMO+2	nπ* + $\pi\pi$*
T$_4$	HOMO	→	LUMO+3	nπ* + $\pi\pi$*
T$_5$	HOMO	→	LUMO+4	nπ* + $\pi\pi$*
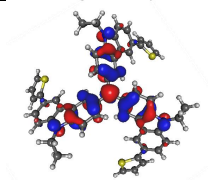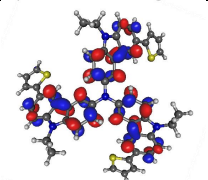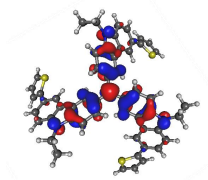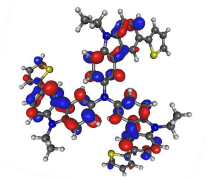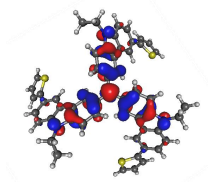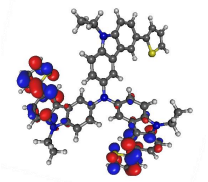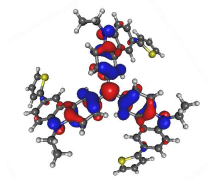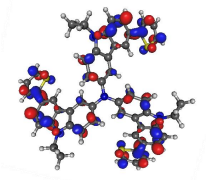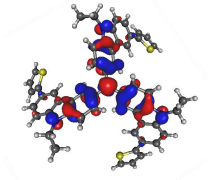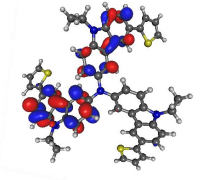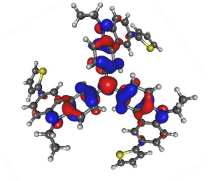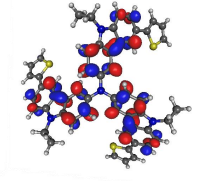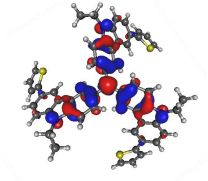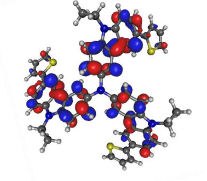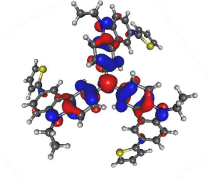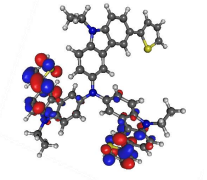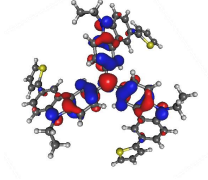
Figure S24. Calculated energy levels of **ThTCA**.

Table S5. Summary of excited states in **ThTCA**

State	Transition		State character
S_1	HOMO	→ LUMO	$n\pi^* + \pi\pi^*$
S_2	HOMO	→ LUMO+1	$n\pi^* + \pi\pi^*$
S_3	HOMO	→ LUMO+2	$n\pi^* + \pi\pi^*$
S_4	HOMO	→ LUMO+3	$n\pi^* + \pi\pi^*$

|				
S$_5$	HOMO	→	LUMO+4	nπ* + ππ*
T$_1$	HOMO	→	LUMO	nπ* + ππ*
T$_2$	HOMO	→	LUMO+1	nπ* + ππ*
T$_3$	HOMO	→	LUMO+2	nπ* + ππ*
T$_4$	HOMO	→	LUMO+3	nπ* + ππ*
T$_5$	HOMO	→	LUMO+4	nπ* + ππ*

7.1 Orbital geometries of TCA HOMO/LUMO levels in ground/excited state structural geometry
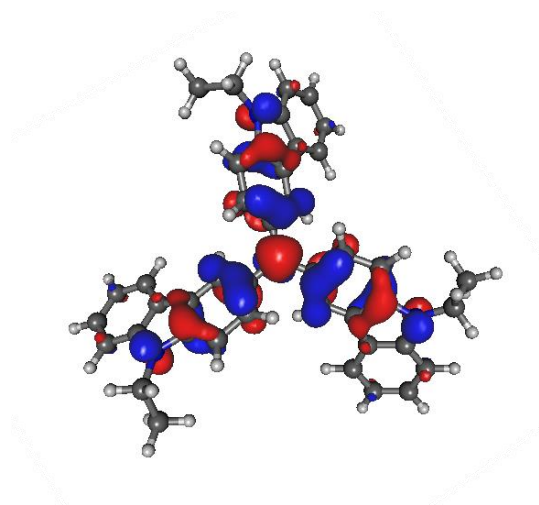
HOMO level of TCA at S_0-state geometry, calculated at DFT/B3LYP/6-31G(d)/PCM(MCH). Isovalue is equal to 0.03 e⁻/au³.
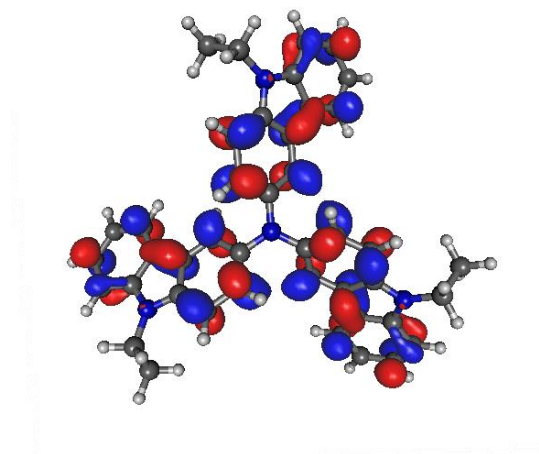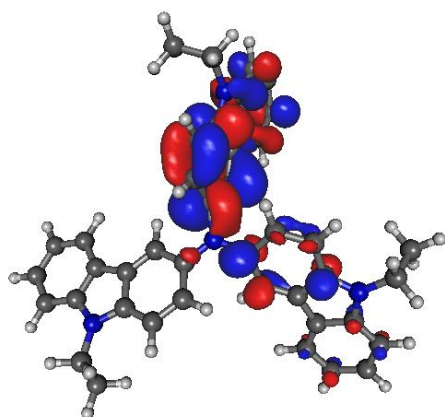

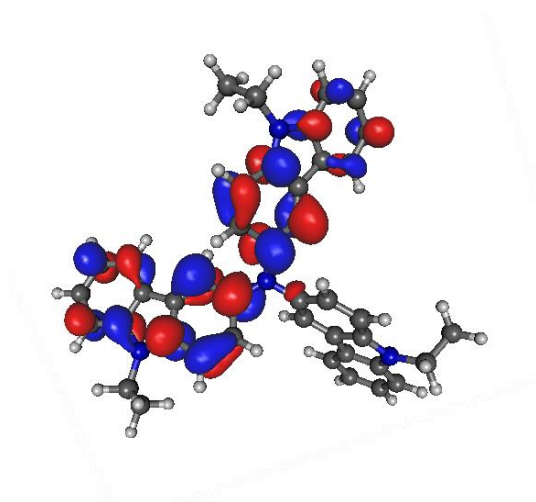LUMO level of TCA at S_1-state geometry, calculated at DFT/B3LYP/6-31G(d)/PCM(MCH). Isovalue is equal to 0.03 e⁻/au³.
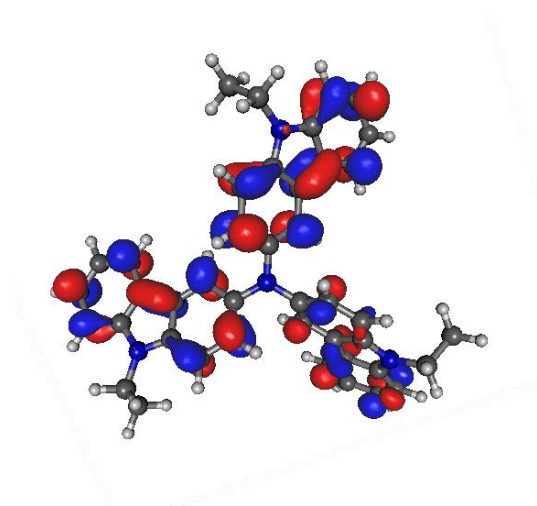
LUMO+1 level of TCA at S_2-state geometry, calculated at DFT/B3LYP/6-31G(d)/PCM(MCH). Isovalue is equal to 0.03 e⁻/au³.
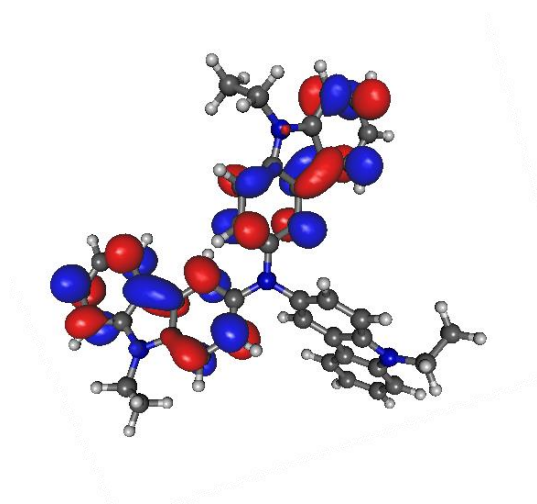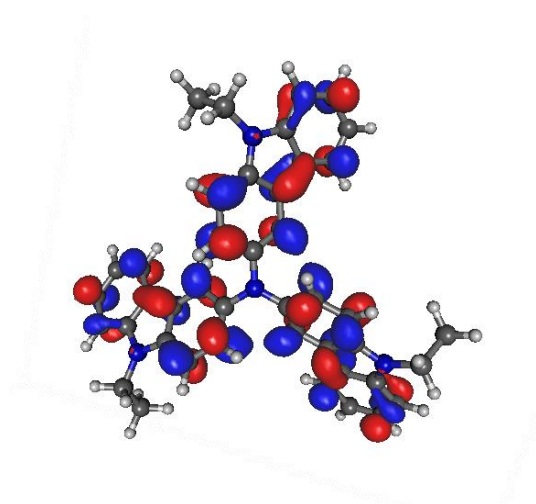

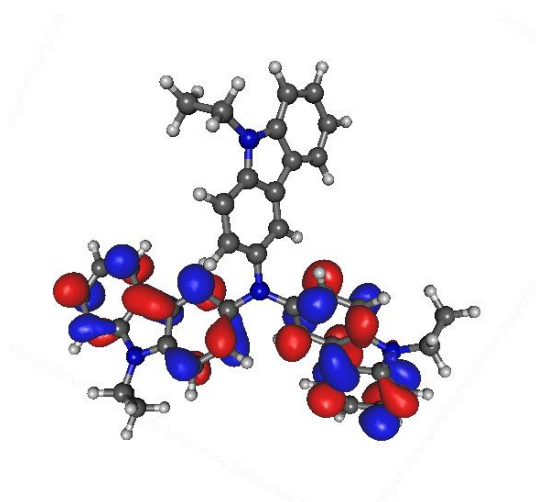LUMO+2 level of TCA at S_3-state geometry, calculated at DFT/B3LYP/6-31G(d)/PCM(MCH). Isovalue is equal to 0.03 e⁻/au³.

LUMO+3 level of TCA at S_4-state geometry, calculated at DFT/B3LYP/6-31G(d)/PCM(MCH). Isovalue is equal to 0.03 e⁻/au³.

LUMO+4 level of TCA at S_5-state geometry, calculated at DFT/B3LYP/6-31G(d)/PCM(MCH). Isovalue is equal to 0.03 e$^-$/au^3.

LUMO level of TCA at T_1-state geometry, calculated at DFT/B3LYP/6-31G(d)/PCM(MCH). Isovalue is equal to 0.03 e$^-$/au^3.

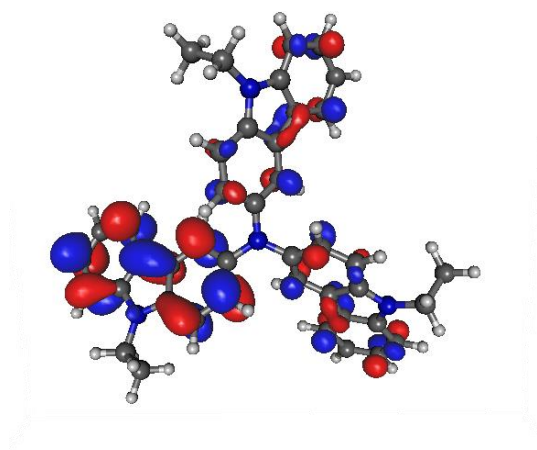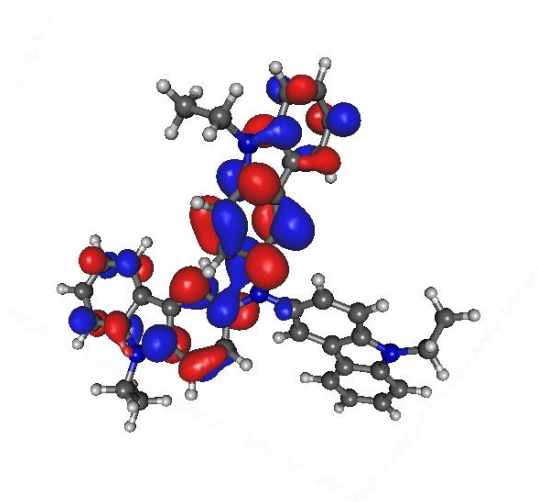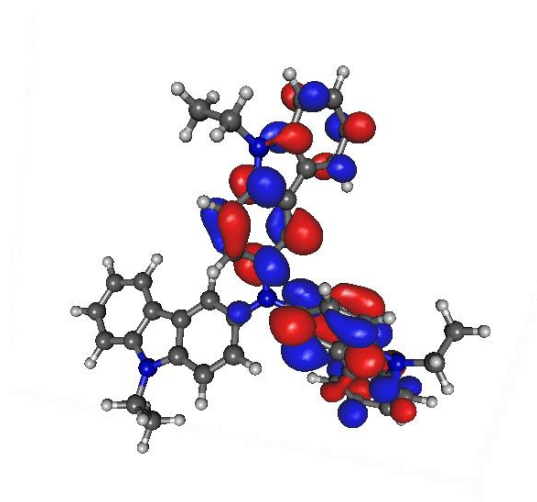LUMO+1 level of TCA at T_2-state geometry, calculated at DFT/B3LYP/6-31G(d)/PCM(MCH). Isovalue is equal to 0.03 e$^-$/au^3.

LUMO+2 level of TCA at T_3-state geometry, calculated at DFT/B3LYP/6-31G(d)/PCM(MCH). Isovalue is equal to 0.03 e$^-$/au^3.

LUMO+3 level of TCA at T_4-state geometry, calculated at DFT/B3LYP/6-31G(d)/PCM(MCH). Isovalue is equal to 0.03 e$^-$/au^3.

LUMO+4 level of TCA at T_5-state geometry, calculated at DFT/B3LYP/6-31G(d)/PCM(MCH). Isovalue is equal to 0.03 e$^-$/au^3.

7.2 Orbital geometries of ThTCA HOMO/LUMO levels in ground/excited state structural geometry
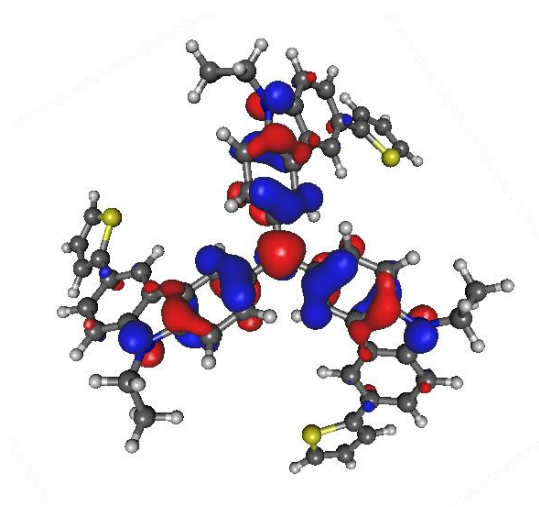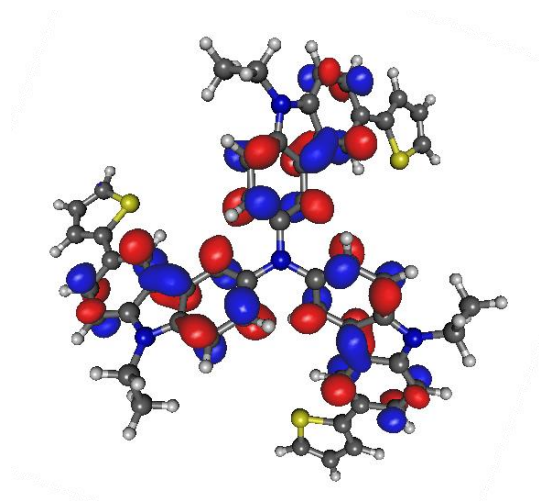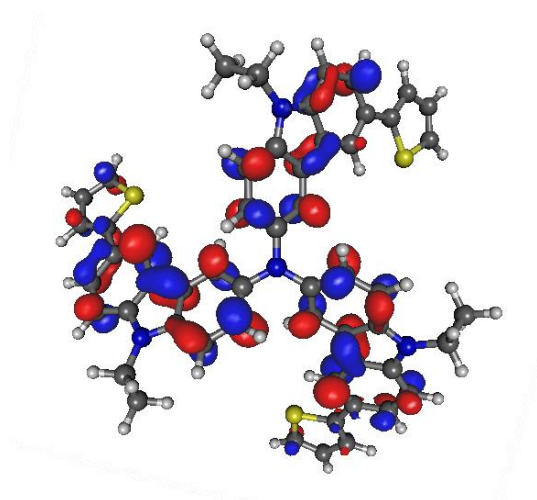

HOMO level of ThTCA at S_0-state geometry, calculated at DFT/B3LYP/6-31G(d)/PCM(MCH). Isovalue is equal to 0.03 e$^-$/au^3.

LUMO level of ThTCA at S_1-state geometry, calculated at DFT/B3LYP/6-31G(d)/PCM(MCH). Isovalue is equal to 0.03 e$^-$/au^3.

LUMO+1 level of ThTCA at S$_2$-state geometry, calculated at DFT/B3LYP/6-31G(d)/PCM(MCH). Isovalue is equal to 0.03 e$^-$/au^3.

LUMO+2 level of ThTCA at S$_3$-state geometry, calculated at DFT/B3LYP/6-31G(d)/PCM(MCH). Isovalue is equal to 0.03 e$^-$/au^3.

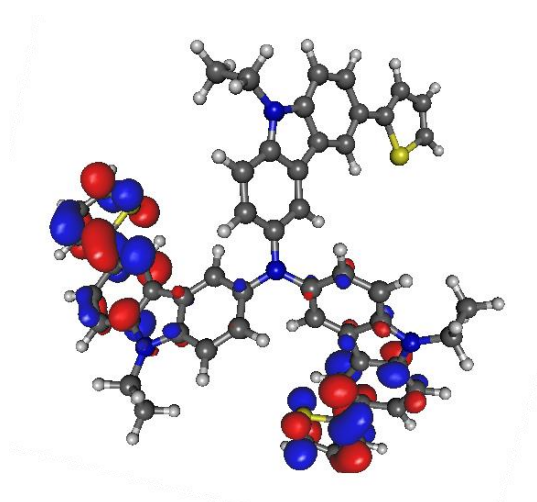LUMO+3 level of ThTCA at S$_4$-state geometry, calculated at DFT/B3LYP/6-31G(d)/PCM(MCH). Isovalue is equal to 0.03 e$^-$/au^3.

LUMO+4 level of ThTCA at S_5-state geometry, calculated at DFT/B3LYP/6-31G(d)/PCM(MCH). Isovalue is equal to 0.03 e⁻/au³.

LUMO level of ThTCA at T_1-state geometry, calculated at DFT/B3LYP/6-31G(d)/PCM(MCH). Isovalue is equal to 0.03 e⁻/au³.
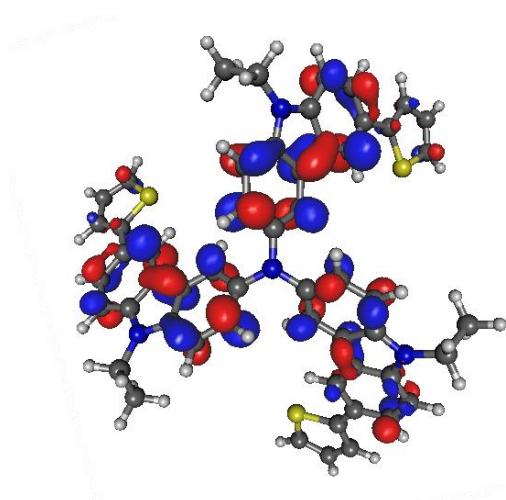
LUMO+1 level of ThTCA at T_2-state geometry, calculated at DFT/B3LYP/6-31G(d)/PCM(MCH). Isovalue is equal to 0.03 e⁻/au³.
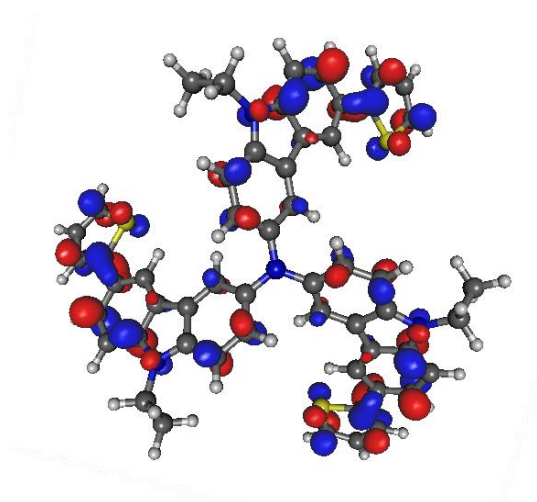
LUMO+2 level of ThTCA at T$_3$-state geometry, calculated at DFT/B3LYP/6-31G(d)/PCM(MCH). Isovalue is equal to 0.03 e$^-$/au^3.
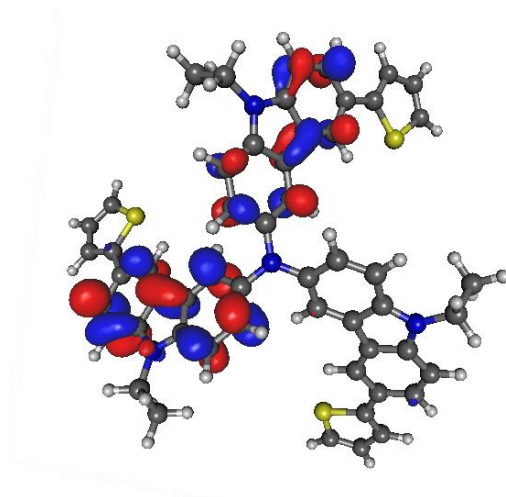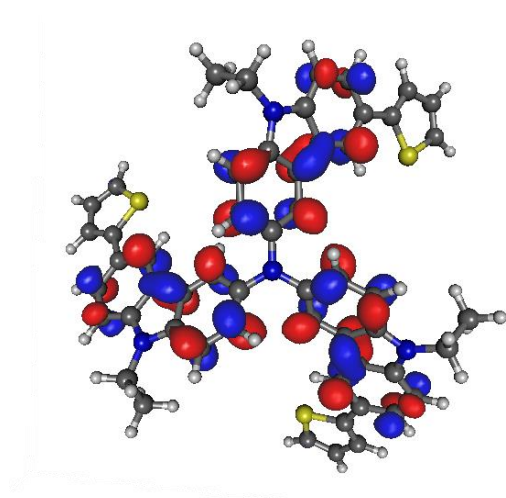

LUMO+3 level of ThTCA at T$_4$-state geometry, calculated at DFT/B3LYP/6-31G(d)/PCM(MCH). Isovalue is equal to 0.03 e$^-$/au^3.

LUMO+4 level of ThTCA at T$_5$-state geometry, calculated at DFT/B3LYP/6-31G(d)/PCM(MCH). Isovalue is equal to 0.03 e$^-$/au^3.

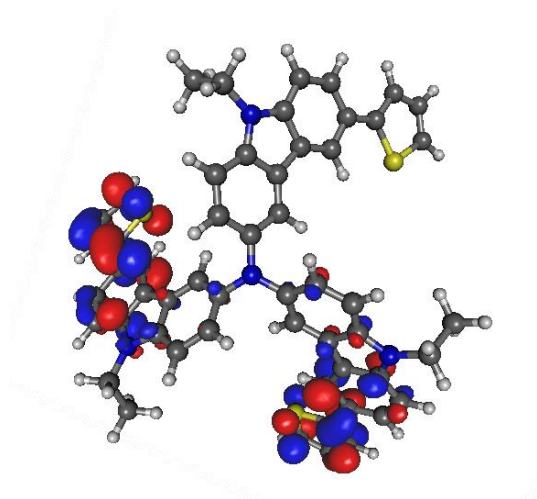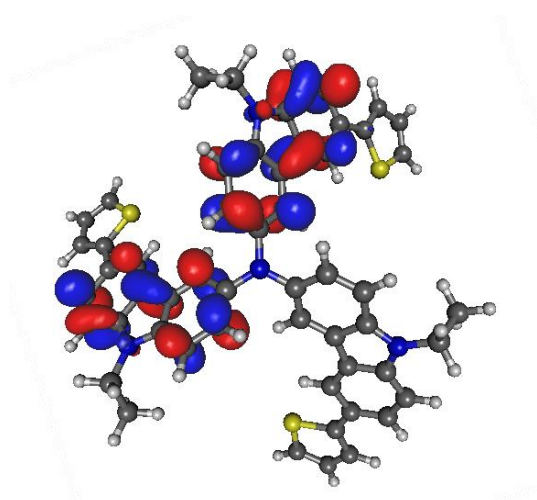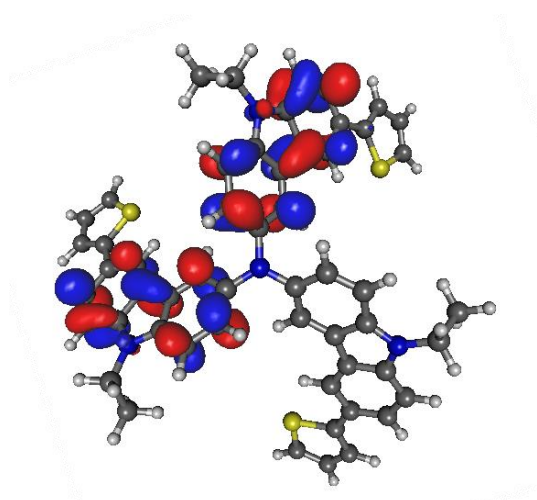## 7.3 Alternative approach

We performed ab-initio density functional calculations based on a model for the molecular core structure, that is fully representative of the entire system. The modeling consists in considering only the methyl-functionalized carbazole MFC linked moieties, while the long alkyl residues R were substituted by CH_3 terminals (see **Figure S25**).

Reliable structures were obtained at the Density Functional Theory (DFT) level and excited states properties were calculated by time-dependent DFT (TDDFT).[S8,S9] For the calculation of vibrational properties,[S10] we adopted a restricted Gaussian basis set 6-31g using the PBE functional,[S11,S12] while for TDDFT calculations the singlet and triplet energies were obtained using the Gaussian09 package[S7] adopting the PBE0 functional[S13,S14] and triple-zeta cc-pVTZ Dunning's basis sets.

We show in **Figure S25** the representation of the model core molecule, which we can see carries an inherent chiral symmetry, and we show also the main vibrational mode chosen for the excited states simulation: it keeps the chiral symmetry and is the first to involve torsion of the MC moieties with respect to the moiety axes.
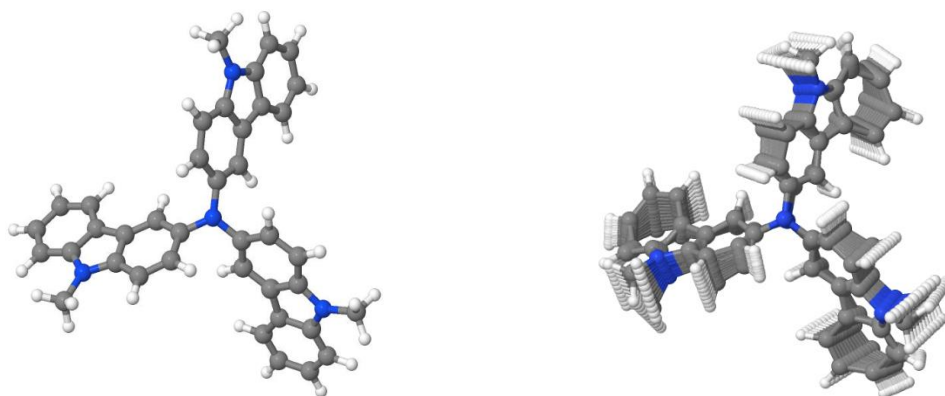

Figure S25. Core molecule model, chiral symmetry structure (left). The chosen vibrational mode (right) involves torsion of each MFC "blade" around its main axis of linkage to the central N-atom.

The Kohn-Sham density for the higher-lying occupied and lower-lying unoccupied orbitals (around the Highest Occupied Molecular Orbital and Lowest Unoccupied Molecular Orbital

HOMO-LUMO gap) relevant for the optical excitations is shown in **Figure S26**. We can see that for the frontier orbitals present very symmetrically extended charge distributions (which bring the eigenstate degeneracies), and thus we also have degenerate excitations, both for singlet and triplet states, equally space-distributed on the system.
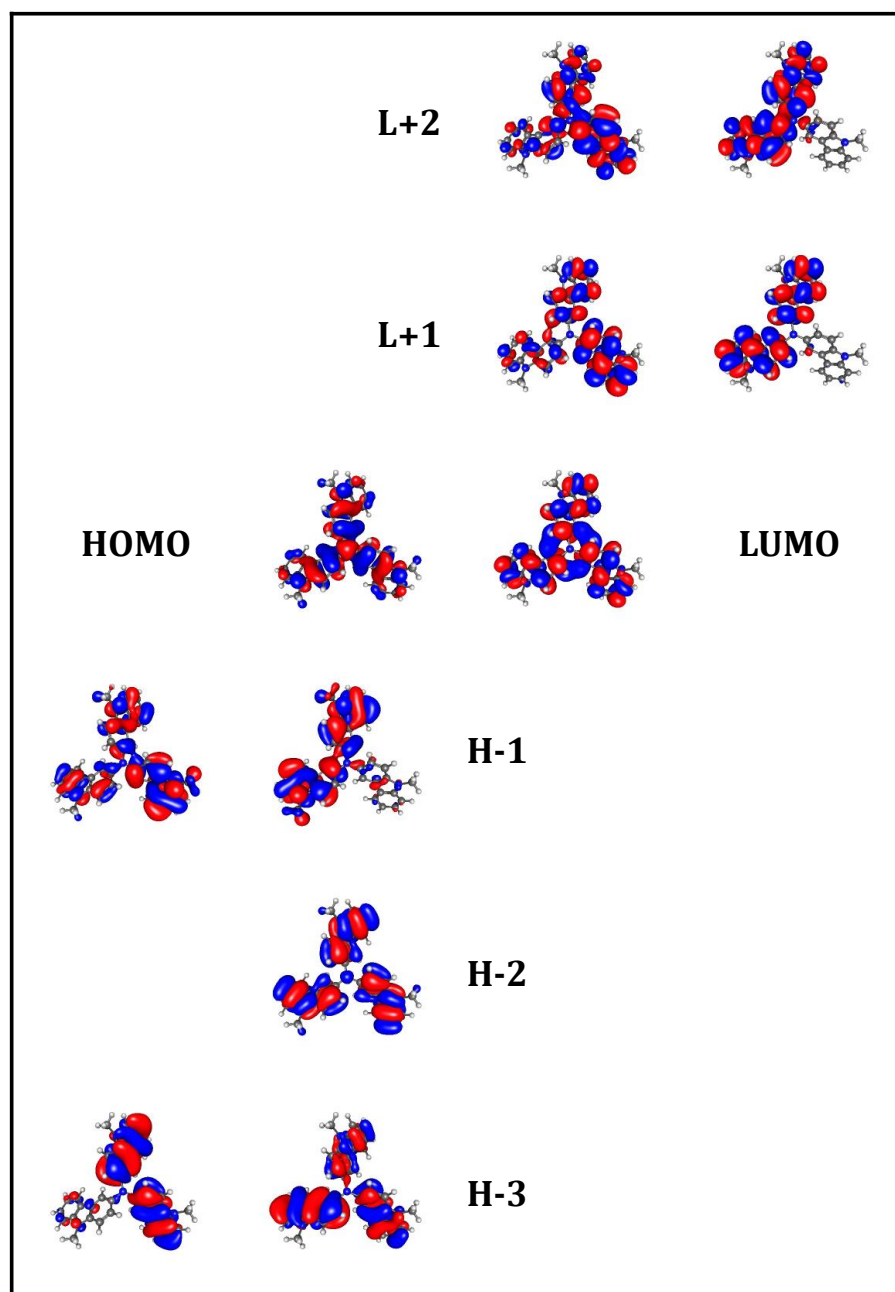
Figure S26. Kohn-Sham orbital density isosurfaces for the states close to the HOMO-LUMO gap; degenerate states are shown side-by-side. Results from computation through Gaussian09, cc-pVTZ basis set.

The excitation energies and their single particle transition contributions, for the ground-state structural conformation, are included in **Table S6**. We find that the first singlet and triplet excited states involve mainly the (homogeneously distributed) HOMO and LUMO orbitals, and

show a sizeable ST splitting of ~0.4 eV. Most relevant here, we find that the first singlet is almost-degenerate with the third triplet state.

We pass now to the joint study of vibrational conformation and electronic excitations, for which we selected the aforementioned mode of symmetric torsion of the MFC moieties with the configurations obtained through the DFT/PBE calculations with the NWChem code.[S10] The resulting frequency for the mode is 25.53 cm^{-1}. We show in **Figure S27** the energy vs configuration coordinate plot for the first excitations in this mode, as calculated through Gaussian09 with the larger basis set (including the energies for the ground state at all configuration coordinates). As seen before in **Table S6**, we will have an ISC inter-system crossing for the first excited singlet to the third excited triplet at the minimum-energy configuration. Other (harder) modes of vibration can then promote reverse crossing in temperature.

Table S6. Excited states for the Chiral Model, singlet S and triplet T spin states. Specified the degeneracy D of each state, the energy in eV (cm^{-1}), the oscillator strength of the excitation OS and the weight C_{IJ} of the main one-electron state transitions involved in the excitation. H, L represent HOMO and LUMO. Calculations were performed by TDDFT at PBE0/cc-pVTZ level.

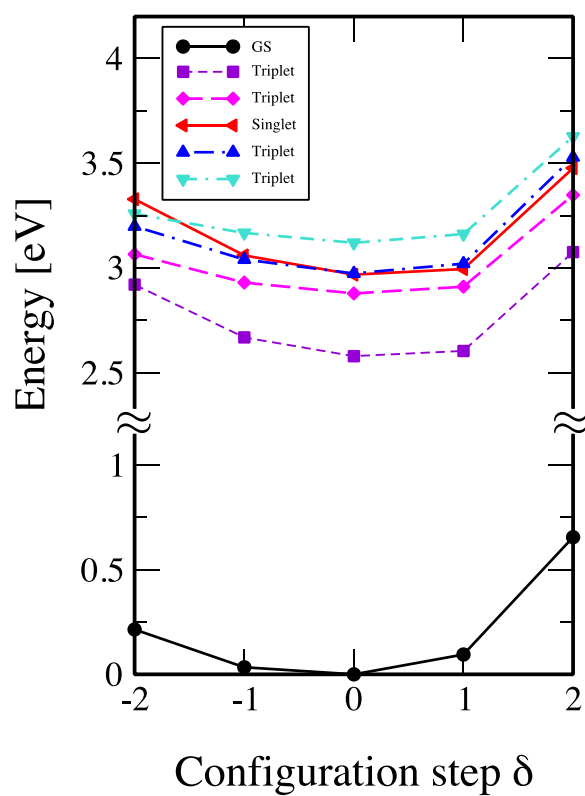| Spin	D	Energy (eV)	Wavelength (nm)	OS	Main transitions ($C_{IJ} \geq 0.25$)
T	single	2.578	480.9	0	H→L (0.67)
T	double	2.877	430.9	0	H→L+1 (0.59) / H→L+1' (0.59)
S	single	2.967	417.9	0.025	H→L (0.7)
T	double	2.973	417.0	0	H→L+2 (0.30) / H→L+2' (0.30) H-3→L (0.26) / H-3'→L (0.26)
T	single	3.119	397.5	0	H-2→L (0.3) H-3→L+1 (0.26) / H-3'→L+1' (0.26)
S	double	3.350	369.0	0.017	H→L+1 (0.69) / H→L+1' (0.69)

Figure S27. Configuration coordinates diagram for the ground state (GS) and lower singlet and triplet excited states of the core molecule model, C3 symmetry chiral conformation.

8. References:

(S1)   Michaleviciute, A.; Gurskyte, E.; Volyniuk, D. Y.; Cherpak, V. V.; Sini, G.; Stakhira, P. Y.; Grazulevicius, J. V. Star-Shaped Carbazole Derivatives for Bilayer White Organic Light-Emitting Diodes Combining Emission from Both Excitons and Exciplexes. *J. Phys. Chem. C* **2012**, *116*, 20769–20778.

(S2)   Kaya, I.; Koyuncu, S. Synthesis and Characterization of Imine-Coupled Polyphenols Containing Carbazole Units. *J. Appl. Polym. Sci.* **2009**, *113*, 1975–1985.

(S3)   Brzeczek, A.; Ledwon, P.; Data, P.; Zassowski, P.; Golba, S.; Walczak, K.; Lapkowski, M. Synthesis and Properties of 1,3,5-Tricarbazolylbenzenes with Star-Shaped Architecture. *Dye. Pigment.* **2015**, *113*, 640–648.

(S4)   Easton, R. E.; Giesen, D. J.; Welch, A.; Cramer, C. J.; Truhlar, D. G. The MIDI! Basis Set for Quantum Mechanical Calculations of Molecular Geometries and Partial Charges. *Theor. Chim. Acta* **1996**, *93*, 281–301.

(S5)   Lynch, B. J.; Truhlar, D. G. Small Basis Sets for Calculations of Barrier Heights, Energies of Reaction, Electron Affinities, Geometries, and Dipole Moments. *Theor. Chem. Acc.* **2004**, *111*, 335–344.

(S6)   Allouche, A.-R. Gabedit-A Graphical User Interface for Computational Chemistry Softwares. *J. Comput. Chem.* **2011**, *32*, 174–182.

(S7)   M.J. Frisch, G.W. Trucks, H.B. Schlegel, G.E. Scuseria, M.A. Robb, J.R. Cheeseman, G. Scalmani, V. Barone, B. Mennucci, G.A. Petersson, H. Nakatsuji, M. Caricato, X. Li, H.P. Hratchian, A.F. Izmaylov, J. Bloino, G. Zheng, J.L. Sonnenberg, M. Hada, M. Ehara, K. Toyota, R. Fukuda, J. Hasegawa, M. Ishida, T. Nakajima, Y. Honda, O. Kitao, H. Nakai, T. Vreven, J.A. Montgomery, Jr., J.E. Peralta, F. Ogliaro, M. Bearpark, J.J. Heyd, E. Brothers, K.N. Kudin, V.N. Staroverov, R. Kobayashi, J. Normand, K. Raghavachari, A. Rendell, J.C. Burant, S.S. Iyengar, J. Tomasi, M. Cossi, N. Rega, J.M. Millam, M. Klene, J.E. Knox, J.B. Cross, V. Bakken, C. Adamo, J. Jaramillo, R. Gomperts, R.E. Stratmann, O. Yazyev, A.J. Austin, R. Cammi, C. Pomelli, J.W. Ochterski, R.L. Martin, K. Morokuma, V.G. Zakrzewski, G.A. Voth, P. Salvador, J.J. Dannenberg, S. Dapprich, A.D. Daniels, O. Farkas, J.B. Foresman, J.V. Ortiz, J. Cioslowski, D.J. Fox, Gaussian 09, revision A.1; Gaussian, Inc. (2009), Wallingford, CT.

(S8)   Runge, E.; Gross, E. K. U. Density-Functional Theory for Time-Dependent Systems. *Phys. Rev. Lett.* **1984**, *52*, 997–1000.

(S9)   C. A. Ullrich, "Time-dependent density-functional theory: concepts and applications" OUP Oxford (2011).

(S10)   Valiev, M.; Bylaska, E. J.; Govind, N.; Kowalski, K.; Straatsma, T. P.; Van Dam, H. J. J.; Wang, D.; Nieplocha, J.; Apra, E.; Windus, T. L.; de Jong, W. A. NWChem: A Comprehensive and Scalable Open-Source Solution for Large Scale Molecular Simulations. *Comput. Phys. Commun.* **2010**, *181*, 1477–1489.

(S11)   Perdew, J. P.; Burke, K.; Ernzerhof, M. Generalized Gradient Approximation Made Simple. *Phys. Rev. Lett.* **1996**, *77*, 3865–3868.

(S12)   Perdew, J. P.; Burke, K.; Ernzerhof, M. Generalized Gradient Approximation Made Simple [Phys. Rev. Lett. 77, 3865 (1996)]. *Phys. Rev. Lett.* **1997**, *78*, 1396–1396.

(S13)   Perdew, J. P.; Ernzerhof, M.; Burke, K. Rationale for Mixing Exact Exchange with Density Functional Approximations. *J. Chem. Phys.* **1996**, *105*, 9982–9985.

(S14)   Adamo, C.; Barone, V. Toward Reliable Density Functional Methods without Adjustable Parameters: The PBE0 Model. *J. Chem. Phys.* **1999**, *110*, 6158–6170.